ISTANBUL TECHNICAL UNIVERSITY ★ GRADUATE SCHOOL OF SCIENCE ENGINEERING AND TECHNOLOGY

COMPUTATIONAL INVESTIGATION OF METAL-PROTEIN INTERACTIONS IN YEAST FOR BIONANOTECHNOLOGY

M.Sc. THESIS

Erhan ÖZDAMAR

Department of Nano Science and Nano Engineering

Nano Science and Nano Engineering Programme

JANUARY 2013

ISTANBUL TECHNICAL UNIVERSITY ★ GRADUATE SCHOOL OF SCIENCE ENGINEERING AND TECHNOLOGY

COMPUTATIONAL INVESTIGATION OF METAL-PROTEIN INTERACTIONS IN YEAST FOR BIONANOTECHNOLOGY

M.Sc. THESIS

Erhan ÖZDAMAR
(513101029)

Department of Nano Science and Nano Engineering

Nano Science and Nano Engineering Programme

Thesis Advisor: Assist. Prof. Dr. Bülent BALTA

Co-advisor: Prof. Dr. Zeynep Petek ÇAKAR

JANUARY 2013

İSTANBUL TEKNİK ÜNİVERSİTESİ ★ FEN BİLİMLERİ ENSTİTÜSÜ

MAYADA METAL-PROTEİN ETKİLEŞİMLERİNİN BİYONANOTEKNOLOJİ İÇİN HESAPSAL OLARAK İNCELENMESİ

YÜKSEK LİSANS TEZİ

Erhan ÖZDAMAR
(513101029)

Nano Bilim ve Nano Mühendislik Anabilim Dalı

Nano Bilim ve Nano Mühendislik Yüksek Lisans Programı

Tez Danışmanı: Yrd. Doç. Dr. Bülent BALTA

Eş Danışmanı: Prof. Dr. Zeynep Petek ÇAKAR

OCAK 2013

Erhan Özdamar, a **M.Sc.** student of ITU **Graduate School of Science, Engineering and Technology,** student ID **513101029**, successfully defended the **thesis/dissertation** entitled "**COMPUTATIONAL INVESTIGATION OF METAL-PROTEIN INTERACTIONS IN YEAST FOR BIONANOTECH-NOLOGY**", which he prepared after fulfilling the requirements specified in the associated legislations, before the jury whose signatures are below.

Thesis Advisor :	**Assist. Prof. Dr. Bülent BALTA** İstanbul Technical University	....
Co-advisor :	**Prof. Dr. Zeynep Petek ÇAKAR** İstanbul Technical University	....
Jury Members :	**Prof. Dr. Safiye SAĞ ERDEM** Marmara University	....
	Assoc. Prof. Dr. Fatma Neşe KÖK İstanbul Technical University	....
	Assoc. Prof. Dr. Alimet Sema ÖZEN Piri Reis University	....

Date of Submission : 17 December 2012
Date of Defense : 24 January 2013

To my spouse,

FOREWORD

First of all, I would like to thank my thesis advisor Assist. Prof. Dr. Bülent Balta for his incredible patience, understanding and for precious helps and guidance.
And also, I wish to express my sincere gratitude to my co-advisor Prof. Dr. Zeynep Petek Çakar for her helps, motivations and supports.
In addition, I acknowledge the financial support of the Scientific and Technological Research Council of Turkey (TUBITAK BIDEB-2210) during my whole graduation study. And also this work was supported in part by TUBITAK (project number 109T6380), COST-Action (CM0902), and the National Center for High Performance Computing of Turkey (UYBHM) under the grant number 4001492011.
Moreover, I thank my lab partner Aydın Özmaldar for his helps and motivations during my thesis project. Also, I'd like to thank my dear friend Mümin Balaban for his supports, motivations and precious friendship.
And finally, but most importantly, I'd like to thank to my beloved wife for all the support, the patience and the unending love.

December 2012 Erhan ÖZDAMAR

TABLE OF CONTENTS

Page

ABBREVIATIONS

AF	: Antiferromagnetic coupling
Ala/A	: Alanine
Asp/D	: Aspartate
Co	: Cobalt
Cu	: Copper
CueO	: Cuprous efflux oxidase
Cys/C	: Cysteine
DFT	: Density functional theory
$\mathbf{E_{xc}}$	: Exchange-correlation energy
ET	: Electron transfer
FC	: Ferromagnetic coupling
Fe	: Iron
FR	: Fully reduced
$\mathbf{H_2O}$	: Water
hCp	: Human Ceruloplasmin
HF	: Hartree Fock
His/H	: Histidine
GGA	: Generalized Gradient Approximation
Glu/E	: Glutamate
KS	: Kohn Sham
LDA	: Local Density Approximation
MCO	: Multi-Copper Oxidase
MM	: Molecular mechanics
NI	: Native intermediate
Ni	: Nickel
$\mathbf{O_2}$	: Dioxygen
ONIOM	: Our own N-layered Integrated molecular Orbital and molecular Mechanics
PI	: Peroxy intermediate
r	: Radial distance
RO	: Resting oxidized
QM	: Quantum mechanics
V	: Potential energy
T	: Kinetic energy
TNC	: Tri-nuclear copper cluster
UEG	: Uniform electron gas
Z	: Atomic number
$\hat{\mathbf{H}}$	: Hamiltonian
$\boldsymbol{\rho}(\mathbf{r})$	: Spin density
ρ_σ	: Spin density
χ_σ	: Reduced spin density
τ_σ	: Spin kinetic energy density
ψ	: Wave function

LIST OF TABLES

Page

LIST OF FIGURES

Page

COMPUTATIONAL INVESTIGATION OF METAL-PROTEIN INTERACTIONS IN YEAST FOR BIONANOTECHNOLOGY

SUMMARY

Fet3p is a multicopper oxidase protein found in yeast, *Saccharomyces cerevisiae* and responsible for the high affinity iron uptake into the cell. It is a membrane-bound protein and in complex with the Ftr1p protein. Fet3p reduces O_2 into H_2O by 4 substrate (iron) oxidations. Then the oxidized iron ions are transferred to Ftr1p, and Ftr1p transports the iron ions into the cell. In addition to the ferroxidase activity, the enzyme also shows cuprous oxidase activity.

The enzyme has four copper cofactors in three types: T1, T2 and T3. All cofactor copper ions are in +1 state, at the beginning. Then the dioxygen comes and binds to the trinuclear copper cluster (formed by T2 and T3 coppers). The reduction of the O_2 and the cleavage of the O-O bond occur by taking one electron from each copper ion. After dioxygen cleavage, the cofactor copper ions are in the +2 state. In order to return to the starting structure, 4 iron oxidations coupled with copper reductions occur. During these reactions, 4 protons come from the environment and the reduction derivatives of the dioxygen are converted to water.

In the literature, there are bunch of informations about the reduction of dioxygen. However, from that point, the copper ion reductions by iron oxidations and protonations of the oxygen derivatives are not studied before. Therefore, these unstudied reactions and the order of these reactions are the interest of this study.

The reactions are investigated computationally with quantum mechanics/molecular mechanics methods (QM/MM). M06-2X is the chosen density functional method for this study. The results show that the reactions do not seem the happen without any protonations. A possible mechanism of the reactions is proposed as follows: First a protonation occurs then a substrate oxidation occurs and this cycle repeats 4 times.

On the other hand, in yeast, Fet3p contributes to resistance to transtion metal stresses other than Fe^{+2}. In order to determine whether Fet3p can oxidize other transiton metals as well, Fe^{+2} has been replaced with Cu^{+}, Co^{+2} and Ni^{+2} and the reaction energies have been calculated. Consistent with experiments, Fet3p oxidizes Cu^{+} ion to a less toxic form, Cu^{+2}. On the other hand, the enzyme oxidizes cobalt ions only under extremly low pH conditions. In the case of nickel as the substrate, Fet3p cannot oxidize the substrate. Thus, the resistance mechanism for Co and Ni, does not involve oxidation of these metals.

MAYADA METAL-PROTEİN ETKİLEŞİMLERİNİN BİYONANOTEKNOLOJİ İÇİN HESAPSAL OLARAK İNCELENMESİ

ÖZET

Fet3p bir çoklu-bakır oksidaz enzimi olup, ekmek mayası olan *Saccharomyces cerevisiae*'da hücre içerisine yüksek afinitede demir alımında rol alır. Fet3p mayanın hücre zarının üzerinde Ftr1p proteini ile birlikte kompleks olarak bulunur. Fet3p dioksijen molekülünü suya indirgerken, aynı zamanda 4 demir(II) iyonunu birer birer yükseltgeyerek Ftr1p proteinine transfer eder. Ftr1p proteini de yükseltgenen demir iyonlarının hücre içerisine taşınmasını gerçekleştirir.

Fet3p proteini kofaktör olarak 4 bakır iyonuna sahiptir. Bu 4 bakır spektroskopik özelliklerine göre 3 tipe ayrılır: T1, T2 ve T3(iki tane). Gerçekleşen reaksiyon döngüsü şu şekilde olmaktadır: Öncelikle, tamamen indirgenmiş yapıda (fully reduced state, bütün bakırlar +1 yüke sahip) dioksijen molekülü T2 ve T3'lerden oluşan üç çekirdekli kümeye(tri-nuclear cluster, TNC) gelir ve bağlanır. Bu aşamada çevresel değişikliklerle ve her bakırdan alınan bir elektron ve ortamdan alınan bir protonla dioksijen, O^{-2} ve OH^{-} iyonlarına parçalanır. Böylece bütün bakırlar +2 durumuna yükseltgenirler ve bu aşamaya doğal ara yapı (native intermediate state) denir. Bu noktadan sonra 4 substrat demir(II) iyonu teker teker gelip birer elektron vererek bakır iyonlarını +1 durumlarına geri indirgerler. Bu demir oksidasyonları işlemleri esnasında ayrıca oksijen türevlerinde 4 protonlanma gerçekleşir ve iki su molekülü oluşur. Böylece tekrar tamamen indirgenmiş yapı elde edilir ve tüm döngü tekrar edilir.

Literetürde tamamen indirgenmiş yapıdan, dioksijen ayrımına kadar olan tepkimeler ayrıntılı bir şekilde çalışılmıştır. Ancak, substrat oksidasyonu ve su oluşumu tepkimeleri daha önce hiç çalışılmamıştır. Bu yüzden bu çalışmanın başlıca amaçlarından biri, bu substrat oksidasyonu tepkimeleri, protonlanma etkileri ve olay sıralarının araştırılmasıdır.

Fet3p proteinin ayrıca bakır(I) iyonlarını da substrat olarak alarak yükseltgediği deneysel olarak gösterilmiştir. Yapılan bakır stres çalışmalarda Fet3p, Cu^{+} iyonlarını daha az toksik olan Cu^{+2} iyonlarına yükseltgemiştir. Ayrıca, mayada yapılan diğer geçiş metal stresi çalışmalarında, Fet3p'nin bu streslere karşı dirençte rol aldığı görülmüştür. Kobalt ve nikel streslerine karşı Fet3p proteinin ekspresyonunun arttığı görülmüştür. Kobalt ve nikel için bu ekpresyon artışının iki nedeni olabilir: Ya bakırda olduğu gibi bu metalleri de yükseltgeyebilir ya da hücre içerisine demir alımını arttırarak bu metallerin demirle etkileşen proteinlerde demirin yerine geçmesini önleyebilir. Bu nedenle, bakır, kobalt ve nikel geçiş metalleri demir substratı ile yer değiştirilerek, Fet3p ile tepkimeye girip yükseltgenip yükseltgenemeyecekleri ve Fet3p proteininin substrat seçiciliğinin belirlenmesi de araştırmanın amaçlarından biridir.

Proteinin iç bölgelerine erişim için T2 ve T3'ler tarafında olmak üzere iki tane solvent kanalı bulunmaktadır. Dioksijen T2 tarafındaki solvent kanalından gelir ve

TNC bölgesine bağlanır. Tepkime sonunda oluşan suların hangi kanaldan ayrıldıkları ise daha önce tespit edilememiştir.
Yapılan bu çalışmada Fet3p'nin doğal ara yapısından başlanmak üzere, başlangıç yapısı olan tamamen indirgenmiş yapıya gelene kadar olan tepkimeler araştırılmıştır. Bunun için kuantum mekaniği/moleküler mekanik (QM/MM) yöntemiyle olası tepkimelerin tepken ve ürün yapıları tasarlanmış ve optimize edilmiştir. Bu tepkimelerde gerçekleşen en önemli değişiklik metal iyonlarının yüklerindeki değişiklik olduğu için uygulanacak olan metodun seçilmesinde iyonizasyon enerjisini hesaplanması etkili faktör olmuştur. Metallerin iyonizasyon enerjisini en iyi şekilde hesaplayan M06-2X metodu optimizasyonlarda kullanılmak üzere seçilen yöntem olmuştur. M06-2X metodu bir hibrit yoğunluk fonksiyonel teori metodudur. Tepkimelerin tepken ve ürünlerinin optimize olmuş yapılarının elde edilmesi için iki aşamalı optimizasyonlar şu şekilde gerçekleştirilmiştir. Tepken ya da ürünün yapısına uygun olacak şekilde, proteinin iki kısmı -bakırlı bölge ve substrat bölgesi- ayrı ayrı optimize edilmiş daha sonra birleştirilip tekrardan optimize edilmiştir. Her bölgenin optimizasyonu esnasında diğer bölgedeki atomların konumları sabit tutulmuştur.
Herhangi bir protonlanma olmaksızın yapılan hesaplarda, demirin protein tarafından yükseltgenme tepkime enerjisi endotermik olarak bulunmuştur. Ancak bir protonlanma gerçekleştiğinde, bu tepkime enerjisi endotermikten ekzotermik tarafa geçmiştir. Yalnızca bir proton eklendiği durumda ikinci substratın geldiği durumun denendiği yapılarda ise ürün yapısı elde edilememiştir. İkinci protonlanma ile ikinci substratın varlığındaki yapılar ise hala hesaplanma aşamasındadır. Üçüncü protonlanma ile üçüncü substratın varlığındaki yapılarda ise tepkime enerjisi ekzotermik olarak hesaplanmıştır. Üçüncü protonlamada dördüncü substratın tepken ve ürün yapısı elde edilmiş ve hesaplanan reaksiyon enerjisi endotermik olarak heaplanmıştır. Dördüncü protonlanma durumunda dördüncü substratın yükseltgenme tepkime enerjisi ise endotermik olarak hesaplanmıştır. Elde edilen verilere bakılarak, tepkimelerin şu şekilde gerçekleştiği düşünülmektedir: Önce bir protonlanma gerçekleşir, ardından bir substrat yükseltgenmesi meydana gelir. Bu döngü 4 defa tekrar ederek doğal ara yapıdan başlangıç yapısı olan tamamen indirgenmiş yapıya geri dönülür. Bu esnada gerçekleşen protonlanmalar sayesinde 2 su molekülü oluşur ve sistemi T3'ler tarafındaki solvent kanallarından terk ederler.
Yapılan optimizasyonlarda, yükseltgenen demir iyonunun indirgenmiş demir iyonuna göre T1'den 0,2Å daha uzakta durduğu saptanmıştır. Demir iyonu yükseltgendikten sonra substrat-bağlanma bölgesinin çıkışına doğru ilerlemektedir. Bunun sebebi ise artan demir yükü ile pozitif bakırlı bölge arasındaki elektriksel itme etkileşiminden kaynaklanmaktadır.
Diğer yandan Fet3p'nin substrat seçiciliğinin belirlenmesi için yapılan hesaplamalarda, Fet3p'nin bakırı da yükseltgediği görülmüştür. Bu sonuç da deneylerle tutarlılık göstermektedir. Hesaplama sonucu, tepkime enerjisi endotermik olarak hesaplanmasına rağmen benzeri demirli tepkime enerjisinden daha düşük enerjili bulunmuştur. Bunun sebeplerinin ise substrat bakırın indirgenmiş haldeyken Fet3p ile yaptığı etkileşimlerin demirden farklı olmasından, özellikle 345 numaralı metiyoninin kükürtüyle etkileşmesinden kaynaklandığı düşünülmüştür.
Kobaltın demir yerine yerleştirilip yapılan hesaplamalarda ise ürün yapısı protonsuz yapılarda elde edilememiş ve dolayısıyla bu tepkimenin gerçekleşmediği düşünülmüştür. Ancak, uç bir durum olarak dizayn edilen, 4 protonlu yapıda ise ilk substrat kobaltın yükseltgendiği görülmüştür. Dolayısıyla, Fet3p'nin ancak uç koşullarda, düşük pH durumlarında kobaltı yükseltgeyebileceği düşünülmüştür.

Ancak aynı yapıda 4. Substratın yükseltgenmediği de görülmüştür. Dolayısıyla bu tepkimenin demirli tepkimelerdeki kadar verimli olmadığı düşünülmüştür.
Nikel demir ile yerdeğiştirildiğinde ise, tepkime gerçekleşmemiştir. Sadece substrat bağlama bölgesinin optimizasyonlarında nikelin +3 olması için yapılan girişimler Ni^{+2} olarak sonuçlanmıştır. Nikel substrat-bağlama bölgesindeki bir glutamattan bir elektron almış ve +2 yapısını oluşturmuştur. Dolayısıyla nikel bakırlar tarafından yükseltgense bile yakınındaki glutamattan bir elektron koparak indirgenmiş yapısına geri dönecektir.
Bu bağlamda, Fet3p, geçiş metalleri stresi koşullarında, bakırı daha az toksik olan formu olan Cu^{+2}'ya yükseltgeyerek katkı yapar. Kobalt stresinde ise, Fet3p ancak düşük pH durumlarında kobaltı +3 haline yükseltger. Nikel stresinde ise Fet3p nikelle tepkimeye girmez.

1. INTRODUCTION

1.1. Biological Importance of Metal Ions

Metals are natural elements of the Earth's crust. They have in general high electrical conductivity, high thermal conductivity and high density [1,2]. Apart from their physical properties, metal ions are important trace elements for living organisms. Furthermore, they have crucial roles in biochemical reactions such as water cleavage during oxygenic photosynthesis, nitrogen fixation, respiration, hydrogen assimilation, and transcription and development of cell. On the other hand, some of these metal ions are used as cofactors while others have some functional and structural missions in the cellular metabolism [3]. In addition, metal ions have crucial importance in biotechnology, especially in nanobiotechnology, biomaterials and biomimetics. In biomaterials, for the integration of the implant with the tissue, the adsorption of protein is the most crucial criteria. In the case of nanobiotechnology, the protein-surface interactions form the basis for the functional biological/ electronical devices like sensors and activators. In addition, in biomimetics, the nature is mimicked in order to obtain new designs with novel properties [4].

1.2. Industrial Applications of Metals

Metals are indispensable elements of the industry. They are used widely in all of the industrial areas. For example, iron is used mainly in steel industry [5]; cobalt is used in production and refining of alloys, in jet engines, in gas turbines, in electrochemical materials, as permanent magnets and in varnishes, paints, catalysts, inks, pigments, ceramics and surgical implants [6]; copper is widely used in wire and cable production, in electric motors, in copper pipes, as antimicrobial agent and as wood preservative [7]; whereas nickel is used in stainless steel production, nickel electroplatting, battery and accumulator manufacturing, pigments and ceramic industries [7].

On the other hand, due to heavily usage of the metals in industry, the by-products and the leftover metals pollute the air, the soil and the water and threaten the environment. Therefore they jeopardize the living organisim since they are dangerous to them in excessive concetrations. They cannot be degraded nor destroyed and tend to bioaccumulate in the body. Therefore the remediation of the metal pollution is also important. It can be done not only with environmental remediation tehcniques but also with bioremediation. In bioremediation, the living organisims(micro-organisims and plants, generally) are introduced to the polluted area in order to remove the pollution. Some of the bioremediation techniques are phytoremediation, bioventing, bioleaching, bioaugmentation, rhizofiltration and biostimulation [6].

1.3. Mechanisims of Metal Tolerance in Yeast

One of the essential elements for living organisms is transiton metal ions; however, an imbalance of cellular levels of transition metals can result in toxicity because of the unique redox and coordination properties of these metals. In toxic levels, these metals can block the functional groups, cause denaturation of the enzymes and generation of reactive oxygen species in the Fenton reactions, catalayzed by transition metals. Moreover, by having the capability of inhibition of membrane-bound enzymes on high concentrations, metals can cause distruptions on cellular functions, cellular metabolism and signal transductions [5]. On the other hand, antioxidant molecules like glutathione(GSH) are directly related to the metal ion toxicity. These kind of molecules prevent the metal ion toxicity and a depletion of these molecules result in metal ion toxicity [8].

The baker's yeast or the brewer's yeast *Saccharomyces cerevisia* is perhaps the most useful organism for study of cellular metabolism. Most of the pathways and genes in yeast are higly conserved in higher eukaryotes, even in humans. The yeast genome can be probed for studying metabolism of transition metals by using vast wealth of tools and resources set up by the yeast community. Then, the obtained findings can be extended to study of human homologs [8].

When the metal ions are abundant in the environment, the yeast *Saccharomyces cerevisia* show a resistance to these environmental change to survive by triggering some mechanisms. In general, under metal stress conditions, main resistance mechanisms of yeast are reduction in metal uptake, adsorption(biosorption), efflux pumps(export toxic ions out of the cell membrane), metal sequesteration by metallothioneins, polyphosphates in and /or around the cell and metal detoxification by chelator molecules such as GSH and subsequent transport into the vacuole. Yeast vacuole has a crucial role in metal ion homeostasis and metal ion toxicity by storing metal ions. Vacuoles creates electrochemical potential by using proton pumps allowing cation transport inside [8].

1.4. The Protein Fet3p

Fet3p is a membrane-bound, protein in yeast and involved in high affinity iron uptake into the cell. It belongs to a protein family called multicopper oxidases (MCO). Multicopper oxidases are a family of enzymes that primarily reduce dioxygen (O_2) to water (H_2O) by oxidizing a broad range of substrates from organics to inorganics. They are found all organisms from bacteria to yeast and from plants to animals. Some of the well-known examples of this family are plant laccases that are responsible for lignin formation; fungal laccases to degrade and to detoxify lignin; cuprous efflux oxidase (CueO) for copper homeostasis in bacteria; human ceruloplasmin (hCp) and Fet3p in yeast mainly responsible for the ferroxidase activity [9-14].

Fet3p, is responsible for the high affinity iron uptake in *Saccharomyces cerevisiae*. Fet3p is also an ortholog to human ceruloplasmin that is involved in transporting iron from organs and tissues to the blood. Fet3p reduces O_2 to H_2O by using Fe^{+2} as substrate and oxidizing it to Fe^{+3}. This enzyme is found on the yeast membrane in a complex with the protein iron permease Ftr1p. Fe^{+2} cannot enter the cell, Ftr1p only transfers Fe^{+3} ion into the cell, that is why the reaction of Fet3p is crucial for the cell. First, Fet3p oxidizes its substrate to Fe^{+3}, and then transfers this product ion to Ftr1p; and Ftr1p transports Fe^{+3} into the cell [15-17].

In addition to its ferroxidase activity, Fet3p also oxidizes Cu^{+} to Cu^{+2}, in order to detoxify the pro-oxidant Cu^{+}, hence it plays a key role in copper homeostasis as well as in iron homeostasis [18-20]. It has been shown that Fet3p is also involved in resistance against stresses caused by transition metals other than Fe^{+2}, like Mn^{+2}, Zn^{+2}, Ni^{+2}, Cu^{+} and Co^{+2} [21,22]. This can be mainly due to two reasons: On some proteins, which are normally, complexed with iron, this metal ion may be replaced by another transition metal ion at high concentration; as a result, the expression of Fet3p may be upregulated, increasing iron uptake. This would favor iron against other transition metal ions in competition to bind to proteins. Secondly, Fet3p may oxidize some of these transition metal ions, and these oxidized ions may be detoxified by a yet unknown mechanism. Probably, the first mechanism acts in the case of Zn^{+2} stress because this ion is not redox active. In the case of Cu^{+} stress, there is experimental evidence that the second mechanism takes place. The mechanisms for the other ions have not been investigated in the literature and are studied in the present work.

On the other hand, Fet3p, being a member of MCO protein family, has the industrial potential to be used in biological fuel cells and in detoxification [23].

To investigate such a biologically and bionanotechnologically important enzyme, first the oxidation mechanism of the actual substrate (iron) has been studied in this study. Then, to investigate the substrate specificity of Fet3p, i.e. whether or not this enzyme can oxidize other transition metals (Co^{+2} and Ni^{+2}), the information obtained from of this iron oxidation mechanism has been used as a starting point. Although Fet3p is already known to be able to oxidize Cu^{+}, this ion has also been included in this work in order to compare its reaction mechanism with that of Fe^{+2}.

Fet3p, as well as other MCOs, couples 4 one-electron oxidations (each electron coming from a different Fe^{+2} in the case of Fet3p) and 4 electron reduction of O_2 to H_2O (Eq. 1.1) [24].

$$4Fe^{+2} + O_2 + 4H^{+} \rightarrow 4Fe^{+3} + 2H_2O \qquad \textbf{(1.1)}$$

The protein has four coppers as cofactors. According to their spectral features, these coppers are classified in three types: T1, T2, and T3 (T3a and T3b). T2 and T3 coppers are located close to each other and are called as the trinuclear cluster (TNC) [24]. The electron transfer (ET) mechanism of Fet3p, as well as other MCOs, occurs mainly in 3 steps shown in Figure1.1. First, dioxygen binds to the TNC and is reduced by taking one electron from each of the coppers. Secondly, the T1Cu site is reduced by the substrate (Fe^{+2} in Fet3p). Thirdly, this electron moves from the T1Cu site to the TNC site and reduces one of the oxidized coppers there. The second and third steps are repeated until all copper sites are reduced and a new substrate is oxidized each time. During this process, 4 protons are taken from the environment and 2 water molecules are produced. To be clear, the main role of the T1Cu is to shuttle electrons from the substrate to the trinuclear cluster site over a distance of nearly 13Å. Some residues play crucial roles on the ET. The electron first moves to the T1Cu by using the connection of carboxylates and the histidines at the substrate-binding site. After that, electron moves to the TNC over the cysteine and histidine between the T1Cu site and TNC site, and oxygen reduction occurs [25,26].

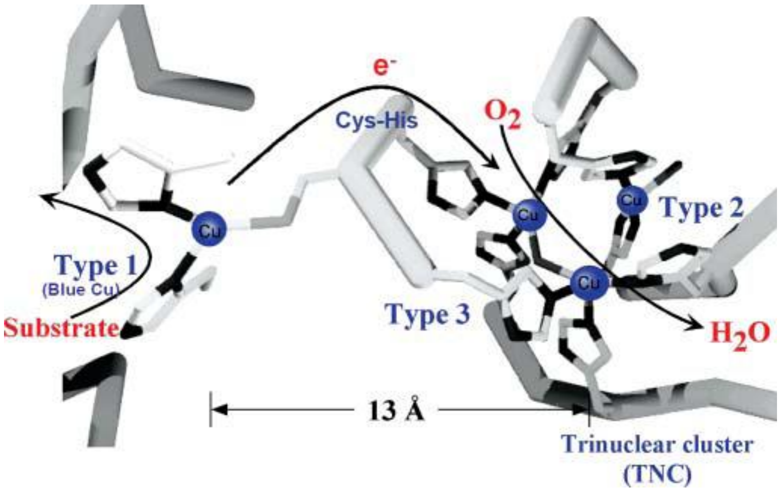

Figure 1.1: Electron transfer pathway from T1Cu site to the TNC [24].

The T1 copper resides near the substrate-binding site; and coordinates with one cysteine (Cys484) and two histidine (His483 and His485) residues. ET from T1 to TNC takes place through C484-H483 and C484-H485. In most of MCO's, there is a weak axial (mostly) methionine ligand, but not in Fet3p. In Fet3p, the side chain of L494 is oriented toward this fourth ligand site and prevents this site from another donor ligand. That is why T1 copper site is in a trigonal planar geometry rather than a trigonal pyramidal one. T1 interacts highly covalently with the sulphur atom of C484; so T1 is responsible for the blue color characterized by the intense Cys-S to Cu charge transfer band at ~600nm. The degree of covalency of the S-Cu interaction varies among the members of the MCO family and is an important factor, which determines the redox potential of T1, a more covalent interaction leading to a higher redox potential [27,28]. On the other hand, T2 copper, the normal copper, resides at the dioxygen-binding site. It is bound to two histidine residues and one water or hydroxide ligand. Lastly, two asymmetric T3 coppers form a binuclear center. In the oxidized form, they show an antiferromagnetic coupling with each other in the presence of a bridging hydroxide ligand (Figure 1.2), and have a characteristic 330nm absorption due to the OH^{-}-Cu^{+2} charge transfer [26,29]. They each have three His ligands. T3 coppers and T2 copper are close to each other and they together form the trinuclear copper center (TNC). Dioxygen binds in the middle of the TNC where it is reduced to water. Oxygen and histidine ligands exhibit a tetrahedral arrangement around the T3 coppers. In TNC site, the 8 His ligands are organized in 4 pairs, each pair exhibiting a very conserved H-X-H motif. This motif helps to stabilize the copper atoms electrostatically [30].

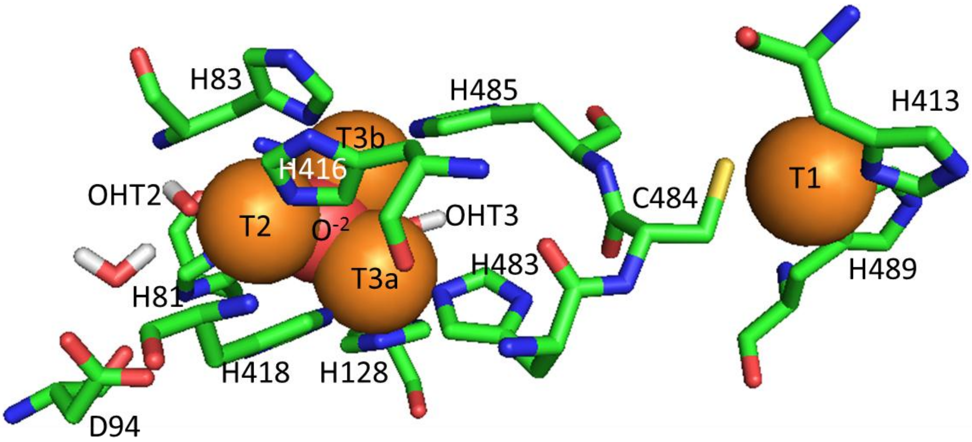

Figure 1.2: Active site of the Fet3p (Green sticks show carbon atoms, while red sticks/spheres stands for the oxygen atoms, grey sticks for hydrogen atoms, navy sticks for the nitrogen atoms and orange spheres for the copper ions).

The substrate binding site of Fet3p is illustrated in Figure 1.3. All of the crystal structures of Fet3p lack the substrate. Therefore, the exact location of the bound Fe substrate is not known. On the other hand, by the help of the mutation studies and the other MCO crystal structures, the amino acids, which are involved in the iron-binding site of Fet3p, are determined. Glutamate-185 (E185), aspartate-409 (D409) and E283 are crucial amino acids for the Fe^{+2} oxidation. Mutations of these amino acids to alanine (A) show an increase in the Michaelis-Menten Km value for Fe^{+2} and a decrease in the ET rate. Therefore, these residues create an excellent environment for high affinity binding of the Fe^{+2}subtsrate. ET from Fe^{+2} to T1 takes place through E185-H489 and D409-H413 interactions [31,32].

The environment of the substrate binding-site of Fet3p is specialized for ferroxidase activity. There are negatively charged, hydrophilic, large carboxylate side chains in the substrate-binding site of Fet3p, which favors Fe^{+2} binding. On the other hand, in laccases, another famous member of the MCO family, this site consists of small and/or nonpolar residues to allow large organic molecules to come in. The mutations of the carboxylates to alanine (E185A/D283A/E409A) in Fet3p result in laccase activity. Therefore, these amino acids have a crucial role in the substrate-specificity of Fet3p for Fe^{+2} rather than neutral organic molecules [33].

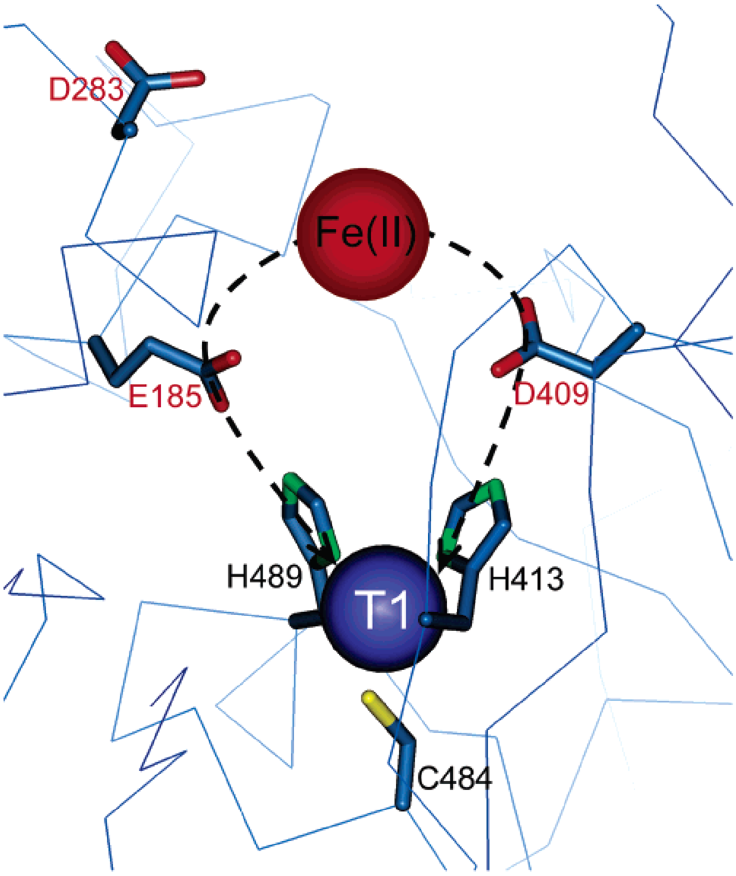

Figure 1.3: Subtrate-binding site of Fet3p [31].

The Figure 1.4 shows the mechanism of dioxygen reduction to water and the intermediates that are formed during this mechanism. In the fully reduced (FR) state, all of the coppers are reduced. Then, the dioxygen binds to the TNC. One of its oxygens bridges the two T3 coppers whereas the other oxygen is oriented toward T2. Next, dioxygen takes two electrons, one from T2 and one from a T3 copper, forming the peroxy intermediate (PI) state. In this state, one of the oxygen atoms of the peroxide interacts with T2 and the other oxygen with one of the T3 coppers. Subsequently, the remaining two coppers are oxidized while peroxide is reduced and the O-O bond is cleaved. This process is facilitated by transferring a proton from E487 to one of the oxygens. The resulting structure is called the native intermediate (NI). In the NI state, all of the coppers are oxidized and there are one O^{-2} and two OH^{-} ions (one comes from the protonation of an oxygen atom formed upon splitting of the dioxygen and the other comes from deprotonation of a water molecule coordinating to T2Cu). Then, four substrate oxidations occur. 4 electrons coming from the oxidations of substrates reduce the Cu^{+2} ions to Cu^{+} and during this process, 4 protons also come from the environment and form two water molecules. So, again the FR state, the starting structure of the mechanism, is formed; and another cycle of the mechanism can begin. A resting oxidized (RO) state has also been observed experimentally. RO is obtained from the NI by taking two protons and forming one water molecule. The conversion of NI to RO is very slow (slower than the enzyme's turnover rate), therefore the actual catalytically relevant fully oxidized form is NI [25,27].

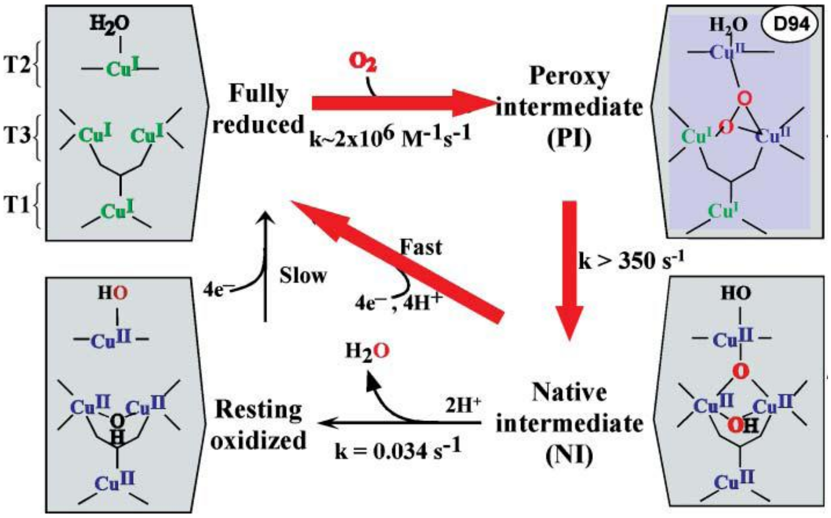

Figure 1.4: Mechanism of O_2 reduction to water by MCOs.

Although the substrate-binding site is closer to the surface, the oxygen-binding active site (TNC site) is buried inside the protein. In the reaction mechanism, one dioxygen molecule binds to the TNC site, and after the reaction, two water molecules go out from this TNC site. To allow passage of the dioxygen and its derivatives, the protein has two solvent access channels. One of these channels leads to the T3Cu sites and the other one to the T2Cu site. The second one is more exposed and more labile than the first one, the dioxygen comes from this channel. However, from which channel the water molecules leave the TNC site is not known yet. These channels are highly conserved in MCOs. It can be said that this solvent channels of MCOs are well suited to allow fast access of O_2 to the TNC and subsequently easy release of water [34,35].

In the second coordination sphere around the TNC site, two important carboxylates are conserved in all archived MCOs: D94 and E487. Residue D94 is located near

T2Cu and T3aCu edge [36,37]. This residue provides a negative charge, which is necessary for the reaction of TNC with the dioxygen and then assists the deprotonation of water ligand of T2Cu during PI to NI decay. The conversion of water to hydroxide creates a negative charge, which stabilizes the oxidized state of T2Cu. On the other hand, E487 is located near the T3 sites, and donates a proton during the reductive cleavage of O-O bond. In short, both residues act together to create a flow of protons to drive the reductive cleavage of the O-O bond and to assist the decay of PI to NI [38,39].

In the literature, many experimental and computational studies enlightened most of the reaction mechanism (Figure1.4); especially from fully reduced structure to the peroxide intermediate and from PI to the native intermediate [15,17,21-24,29-33]. However, the reactions from NI to FR have not been studied before and are still unknown. All that is known is that 4 substrate oxidations (coupled with 4 Cu^{+2} reductions) and 4 protonations occur to produce 2 water molecules and to return to the beginning, fully reduced state. However, from NI to FR state, the sequence of these reactions is undetermined. Do the electrons coming from the substrate oxidation reduce the coppers first and then the protonations occur, or vice versa? Does each substrate oxidation happen after one protonation? To shed light on this complex mechanism, probable structures are computationally studied in this research and a possible mechanism is proposed.

As stated before, Fet3p plays a role in resistance to transition metal stress conditions other than iron. For instance, Fet3p expression is upregulated in the case of cobalt or nickel stresses [22]. That yeast overexpresses Fet3p under transition metal stress conditions might be due to two reasons: to increase the uptake of iron which must compete with the metal causing the stress in some cellular processes or to detoxify other transition metals by oxidizing them (or maybe both). It has been experimentally shown before that Fet3p has also cuprous oxidase activity [18,19]. Therefore, under Cu^{+} stress conditions, Fet3p has a detoxification role and oxidizes Cu^{+} to a less toxic form Cu^{+2}. However, whether or not Fet3p oxidizes other transition metals is not known. Therefore, $Co^{+2}$and Ni^{+2} have been studied as potential substrates for Fet3p to see if they are oxidized or not by Fet3p. Additionally, the oxidation of Cu^{+} as substrate has also been modeled, because experiments suggest that there are a number of differences between the reactions of Fe^{+2} and Cu^{+}. For instance, M345 that is not important in the Fe^{+2} oxidation has a significant role in the Cu^{+} oxidation, whereas E185, which coordinates iron, does not appear to be crucial for copper binding [19].

1.5. Aim of the Study

The aim of this thesis is to investigate what happens between the native intermediate state and the fully reduced state of Fet3p, and the order of these reactions, which was not studied before. And then, by using this information, the substrate specifity of Fet3p is studied with various transition metals; and the results are used to explain the role of Fet3p under transition metal stress conditions in yeast. In addition, the research gives clues about the protein's behavior under different pH conditions. By using the information obtained from this research (substrate specifity, the sequence of substrate oxidation and protonation events and the geometric changes during these reactions), potential mutations of Fet3p can be predicted to increase the substrate specifity or selectivity, and the reaction rate for industrial and bionanotechnological applications. Moreover, in view of the fact that MCOs have very conserved structures, this research sheds light on the reactions of substrate oxidations not only for Fet3p but also for all of the MCOs.

2. MATERIALS AND METHOD

Fet3p geometry optimizations have been carried out with different substrates and with different charges and spin states. The GAUSSIAN09 package has been used for all the geometry optimizations [40]. In order to visualize structures, PyMOL Molecular Visualization program has been used. The starting geometry of Fet3p was taken from the PDB file 1ZPU. Fet3p is a glycoprotein. However, the carbohydrates are on the surface of the protein and do not participate to the reaction; therefore, the carbohydrates have been deleted from that PDB file. This geometry lacks the Fe^{+2} substrate, O^{-2} and 2 OH^{-} ions. But, in the crystal structure of CueO, which is another multicopper oxidase, the substrate, O^{-2} and one of the OH^{-} ions are visible, the substrate being Cu^{+} (PDB code: 1N68). Therefore, the structures of Fet3p and CueO have been aligned, and Fe^{+2}, O^{-2} and OH^{-} have been added to the Fet3p structure according to their positions in CueO. The last OH^{-} has been added manually according to the literature. Then, the protons not resolved in the crystal structure have been added and then a restrained simulation in which everything but the water molecules have been restrained has been done for 500ps. After the simulation, 1490 water molecules and 36 Na^{+} ions, to neutralize the protein, have been kept within the geometry. The van der Waals parameters for Cu, Fe, Co and Ni have been taken from the Babu and Lim's work [41]. For quantum mechanical (QM) calculations, the M06-2X method, a density functional theory (DFT) method, has been used with different basis sets for different atoms. For carbon (C), hydrogen(H), Fe, Co and Ni, the 6-31G basis set; for sulfur (S), nitrogen (N) and O, the 6-31+G basis set; and for Cu an effective core potential basis set CEP-121G have been used. Because the ligands of the coppers and substrates include S, N and O atoms, for these atoms diffuse functions have been used to prevent overestimation of the charge transfers. Since the reactions in Fet3p involve mainly oxidation-reduction reaction, the most important quantity to be calculated accurately is the ionization energy. Therefore, the basis sets for metals and the method have been determined according to benchmark ionization energy calculations (Section 3.1). The Amber force field has been used for the molecular mechanics (MM) calculations [42].

All geometry optimizations have been done at the QM/MM level. The two-layer ONIOM extrapolated scheme has been used as QM/MM approach [43,44]. When a covalent bond between the two layers has been cut, in the calculation of the model region, link atoms have been used to saturate the dangling bonds. Optimizations have been done with mechanical embedding, and micro-iterations have been used during this process. Before each geometry optimization, the stability of the wave function has been checked, and if an instability has been found the wave function has been re-optimized. Cofactor copper ions, imidazoles of His ligands of coppers, O^{-2}, two OH^{-}, the His-Cys-His motif, the Fe^{+2} ion, carboxylate groups of D409 and E185 coordinating to iron, a methionine and a threonine near the substrate-binding site and 4 water molecules (2 at the TNC site and 2 at the substrate-binding site), a total of 186 atoms (upto 189 atoms according to protonation states) form the QM region. Most of the MM region has been kept frozen during geometry optimizations. The optimized MM region consists of the X residues in the H-X-H motif, residues interacting with the QM water molecules at the TNC site, the neighbours of the ligands coordinating with the iron, and the residues (including D283) that are on a loop near the substrate-binding site. The whole QM region has been optimized.

The QM region of the protein has been divided into two parts: the substrate-binding site and the coppers site (TNC and T1 site). These two parts have been optimized first separately, then combined, and optimized again in order to obtain desired product and reactant geometries. For the problematic convergence cases, quadratically convergent SCF procedure (scf=qc) and EDIIS algorithm have been used. Initial geometries for QM/MM optimizations have been taken from the simulaton mentioned above. At the beginning of the optimizations, SCF convergence has been achieved only by using the EDIIS algorithm for the initial iterations, then by switching to the qc algorithm, probably because these initial geometries have been far from the minima. On the other hand, for geometries near the minima, only the default algorithm (a combination of EDIIS and CDIIS) has been used.

2.1 Molecular Mechanics

In the molecular mechanics, the calculations are based on the Newtonian physics. The potential energy is a function of the atomic positions that are generally expressed in Cartesian coordinates. The total potential energy is the sum of bonded and non-bonded energies [45].

$$V(R) = E_{\mathrm{bonded}} + E_{\mathrm{nonbonded}} \qquad \textbf{(2.1)}$$

2.1.1 Bonded energy

Bonded energy contribution consist of mainly three energy elements: bond-stretching angle-bending, and torsion.

$$\mathrm{E_{Bonded}} = \mathrm{E_{bond\text{-}stretch}} + \mathrm{E_{angle\text{-}bending}} + \mathrm{E_{torsion}} \qquad \textbf{(2.2)}$$

Bond-stretching term (Equation 2.3) is defined between two covalently bonded atoms. It indicates the energy arising from the difference of the actual bond length from the ideal bond length.

$$E_{bond-stretch} = \sum_{1,2pairs} \frac{K_b}{2} (b - b_0)^2 \qquad \textbf{(2.3)}$$

The angle-bending term of the equation 2.2 is the harmonic potential due to the difference of the actual angle from the ideal angle between 3 covalently bonded atoms.

$$E_{angle-bend} = \sum_{angles} \frac{K_\theta}{2} (\theta - \theta_0)^2 \qquad \textbf{(2.4)}$$

The torsion term is a cosine function with a symmetry coefficient that comes out from the dihedral angle of 4 atoms that are bonded one to another with a covalent bond [45].

$$E_{torsion} = \sum_{1,4\,pairs} K_\emptyset (1 - \cos(n\emptyset - \gamma)) \qquad \textbf{(2.5)}$$

2.1.2 Non-bonded energy

Non-bonded energy term of the equation 2.1 has two main elements: electrostatic interactions and van der Waals interactions.

$$\mathrm{E_{non\text{-}bonded}} = \mathrm{E_{van\text{-}der\text{-}Waals}} + \mathrm{E_{electrostatic}} \qquad \textbf{(2.6)}$$

The Van der Waals term is calculated by Lennard Jones 12-6 potential.

$$E_{van-der-Waals} = \sum_{nonbonded\,pairs} \left(\frac{A_{ik}}{r_{ik}^{12}} - \frac{C_{ik}}{r_{ik}^{6}} \right) \qquad \textbf{(2.7)}$$

Electrostatic interactions are calculated as coulombic interactions between the charges on the atoms. D is the dielectric constant, q is the charge and the r is the distance between the interacting atoms [45].

$$E_{electrostatic} = \sum_{nonbonded\ pairs} \frac{q_i q_l}{Dr_{ik}} \quad \textbf{(2.8)}$$

2.2 Density Functional Theory And M06-2X

Density functional theory is a quantum mechanical theory. In quantum mechanics, the microscopic systems are described by 'wave functions (Ψ)' that completely characterize all of the physical properties of the system. In QM, the uncertainty principle states that the conjugate variables like position and momentum of an electron cannot be predicted simultaneously with accuracy. Therefore, one can only calculate the probability of an electron in a particular region around the nucleus at a particular time. The position of an electron is described as a probability function Ψ^2. Wave function is not experimentally observable and can be obtained by solving the famous Schrödinger equation (2.9):

$$\hat{H}\,\Psi = E\Psi \quad \textbf{(2.9)}$$

where Ĥ is the Hamiltonian operator of the system, E is the system energy. Ĥ operator includes the kinetic energies of the electrons and nuclei, the attraction of electrons to the nuclei, and interelectronic and internuclear repulsions [46].

As stated above, the wave function is not an experimental observable. In order to work with a physically observable, in DFT, the electron density 'ρ(r)' comes into play. The electron density depends only on the positions and atomic numbers of nuclei and the total number of electrons. The integration of ρ over all space gives N, total number of electrons; and ρ(r) can be also obtained from many-electron wave function Ψ:

$$N = \int p(r)dr \quad \textbf{(2.10)}$$

$$p(r) = N \int \ldots \int \Psi(r_1, r_2 \ldots r_N)^2 ds_1 dr_2 \ldots dr_N \quad \textbf{(2.11)}$$

where d_s is a spin coordinate, d_r's are both spin and spatial coordinates.

Moreover, the nuclei are effective point charges and thus their positions correspond to local maxima in ρ. For each nucleus A located at a ρ maximum $r_{A;}$

$$\left.\frac{\partial \bar{\rho} r_A}{\partial r_A}\right|_{r_A=0} = -2Z_A\rho(r_A) \qquad \textbf{(2.12)}$$

where Z is the atomic number of A, r_A is the radial distance from A and $\bar{\rho}$ is the spherically averaged density.

The density functional theory is based on Thomas Fermi model and the Hohenberg-Kohn theorems. In DFT, electrons interact with each other and with an 'external potential (V_{ext})'. In a molecule, attraction to the nuclei is the external potential. The Hohenberg-Kohn Existence theorem states that external potential is determined by ρ. In other words, there is only one particular distribution of nuclei with their given charges for a given electron density ρ(r).

The second Hohenberg-Kohn theorem is the variational theorem. It states that the ρ obeys the variational principle, which says that the energy evaluated using an approximate density must be greater than or equal to the true ground-state energy. Thus, the energy minimization is done with respect to the electron density.

In Kohn-Sham self-consistent field methodology, the complete ground state energy can be expressed as:

$$E[\rho(r)] = T_{ni}[\rho(r)] + V_{ne}[\rho(r)] + V_{ee}[\rho(r)] + \Delta T[\rho(r)] + \Delta V_{ee}[\rho(r)] \qquad \textbf{(2.13)}$$

where the terms refer, respectively, to the kinetic energy of non-interacting electrons, the nucleus-electron interaction, the classical electron-electron repulsion, the correction to the kinetic energy deriving from the interacting nature of the electrons and all non-classical corrections to the electron-electron repulsion energy.

The kinetic energy is just the sum of the individual electronic kinetic energies for a non-interacting system [46]. Within an orbital expression for the density, Eq. 2.13 can be re-written as:

$$E[\rho(r)] = \sum_i^N \left(\langle \chi_i | -\frac{1}{2}\nabla_i^2 | \chi_i \rangle - \langle \chi_i | \sum_k^{nuclei} \frac{z_k}{|r_i - r_k|} | \chi_i \rangle \right)$$

$$+ \sum_i^N \langle \chi_i | \frac{1}{2} \int \frac{\rho(r')}{|r_i - r'|} dr' | \chi_i \rangle + E_{xc}[\rho(r)] \qquad \textbf{(2.14)}$$

where N is the number of e^-, and $E_{xc}[\rho(r)]$ is the sum of ΔT and ΔV_{ee}. E_{xc} is also known as the exchange-correlation functional. The density for a Slater-determinantal wave function (which is an exact eigen-function for the non-interacting system) is expressed as:

$$\rho = \sum_{i=1}^{N} \langle \chi_i | \chi_i \rangle \qquad \textbf{(2.15)}$$

To find the orbitals χ_i that minimize E;

$$h_i^{KS} \chi_i = \varepsilon_i \chi_i \qquad \textbf{(2.16)}$$

where Kohn-Sham (KS) one-electron operator is expressed as:

$$h_i^{KS} = -\frac{1}{2}\nabla_i^2 - \sum_k^{nuclei} \frac{Z_k}{r_i - r_k} + \int \frac{\rho(r')}{|r_i - r'|} dr' + V_{xc} \qquad \textbf{(2.17)}$$

$$V_{xc} = \frac{\delta E_{xc}}{\delta \rho} \qquad \textbf{(2.18)}$$

V_{xc} is the exchange-correlation potential. It is best described as the one-electron operator for which the expectation value of KS Slater determinant is $E_{xc.}$

E is exact; therefore, the orbital χ must provide the exact density:

$$\sum_{i=1}^{N} h_i^{KS} |\chi_1 \chi_2 \cdots \chi_N\rangle = \sum_{i=1}^{N} \varepsilon_i \, |\chi_1 \chi_2 \cdots \chi_N\rangle \qquad \textbf{(2.19)}$$

KS orbitals are expressed within a basis set of functions (ϕ). The individual ortbital coefficients are determined by solutions of a matrix:

$$F^{KS} \, C = S \, C \, E \qquad \textbf{(2.20)}$$

where C contains the coefficients, S is the overlap matrix, E is the diagonal matrix of orbital energies, and F^{KS} is the Kohn-Sham matrix. The elements of F^{KS} are given by:

$$K_{\mu v} = \langle \phi_\mu \left| -\frac{1}{2}\nabla^2 - \sum_k^{nuclei} \frac{Z_k}{|r - r_k|} + \int \frac{\rho(r')}{|r - r'|} + V_{xc} \right| \phi_v \rangle \qquad \textbf{(2.21)}$$

E_{xc}, in principle, not only includes the difference between the classical and quantum mechanical electron-electron repulsion, but it also accounts for the difference in kinetic energy between the non-interacting system and the real system. The exact form of E_{xc} is not known and the main difference between the DFT methods is $E_{xc.}$ Only for the simple systems, it is possible to derive these functionals; therefore, for other systems approximate forms are derived. The density can be treated locally as a uniform gas (where the density has the same value at every position); this approximation is called as the local density approximation (LDA) [46]. This is a system, in which electrons move in a positive background charge distribution.

On the other hand, in generalized gradient approximation (GGA), in order to improve LDA, a non-uniform gas is considered and the exchange correlation functionals are made dependent not only on the electron density but also on the derivative of the density (i.e. gradient of the density).

In addition, there are hybrid functionals, which include Hartree-Fock exchange in their exchange-correlation functional [46]. The adiabatic connection formula (Eq. 2.22) is expressed as:

$$E_{xc} = (1-a)E_{xc}^{DFT} + aE_{x}^{HF} \quad \textbf{(2.22)}$$

In this thesis, the M06-2X hybrid functional is used. It belongs to the same family with the M06-L, M06 and M06HF. M06 and M06-2X are the re-optimized versions of M05 and M05-2X in the light of the optimizations of M06-L and M06-HF. The main difference between these functionals is the amount of HF exact exchange. M06L is a pure DFT functional; in other words, there is none HF exact exchange, while there is 100% HF exact exchange in M06-HF. For the M06, there is X% HF exact exchange, while M06-2X has 2X% HF exact exchange, where X=27. M06-2X is designed by Zhao et al. and is a hybrid meta-generalized gradient approximation functional. These functionals are used extensively in recent years because of their accuracy, and this accuracy of calculation is based on the exchange-correlation functional, $E\text{xc}[\rho]$ [47].

The local parts of M06 family depend on three variables [48]: spin density (ρ_σ), reduced spin density (x_σ) and spin kinetic energy density (τ_σ).

$$x_\sigma = \frac{|\nabla\rho_\sigma|}{\rho_\sigma{}^{4/3}} \quad \sigma=\alpha,\beta \quad \textbf{(2.23)}$$

$$\tau_\sigma = \frac{1}{2}\sum_{\mathrm{i}}^{\mathrm{occup}} |\nabla\Psi_{\mathrm{i}\sigma}|^2 \quad \textbf{(2.24)}$$

The functionals also have some terms based on the VSXC functional, and these terms have a working variable z_σ and two working functions γ and h:

$$z_\sigma = \frac{2\tau_\sigma}{\rho_\sigma^{5/3}} - C_F, \qquad C_F = \frac{3}{5}(6\pi^2)^{2/3} \quad \textbf{(2.25)}$$

$$\gamma(x_\sigma, z_\sigma) = 1 + \alpha(x_\sigma^2 + z_\sigma) \quad \textbf{(2.26)}$$

$$h(x_\sigma, z_\sigma) = \left(\frac{d_0}{\gamma(x_\sigma,z_\sigma)} + \frac{d_1 x_\sigma^2 + d_2 z_\sigma}{\gamma_\sigma^2(x_\sigma,z_\sigma)} + \frac{d_3 x_\sigma^4 + d_4 x_\sigma^2 z_\sigma + d_5 z_\sigma^2}{\gamma_\sigma^3(x_\sigma,z_\sigma)}\right) \quad \textbf{(2.27)}$$

The exchange functional term ($E_{\mathrm{x}}[\rho]$) of the M06-2X (and also M06) functional is kept same as in the M06-L functional:

$$E_x^{M06} = \sum_\sigma \int dr\left[F_{X_\sigma}^{PBE}(\rho_\sigma, \nabla\rho_\sigma) f(\omega_\sigma) + \varepsilon_{X_\sigma}^{LSDA} h_x(x_\sigma, z_\sigma)\right] \qquad \textbf{(2.28)}$$

where $h_x(x,z)$ is defined in Equation 2.27, $F_{X_\sigma}^{PBE}$ $(\rho_\sigma, \nabla\rho_\sigma)$ indicates the exchange energy density, which is taken from PBE exchange model. $\varepsilon_{X_\sigma}^{LSDA}$ is the the local spin density approximation (LSDA) for exchange, and $f(\omega_\sigma)$ is the spin-kinetic-energy enhancement factor:

$$\varepsilon_{X_\sigma}^{LSDA} = -3/2\left(\frac{3}{4\pi}\right)^{1/3} \rho_\sigma^{4/3} \qquad \textbf{(2.29)}$$

$$f(\omega_\sigma) = \sum_{i=0}^{m} a_i \omega_\sigma^i \qquad \textbf{(2.30)}$$

where the variable ω_σ is the function of t_σ, and the t_σ is the function of spin kinetic energy density (τ_σ) and spin density (ρ_σ).

$$\omega_\sigma = (t_\sigma - 1)/(t_\sigma + 1) \qquad \textbf{(2.31)}$$

$$t_\sigma = \tau_\sigma^{LSDA}/\tau_\sigma \qquad \textbf{(2.32)}$$

where

$$\tau_\sigma^{LSDA} \equiv \frac{3}{10}(6\pi^2)^{2/3}\rho_\sigma^{5/3} \qquad \textbf{(2.33)}$$

Similarly, the functional form of the M06 and M06-2X correlation functionals is identical to the functional form of the M06-L functionals [40]. The opposite-spin and parallel-spin are treated differently.

The opposite-spin M06 correlation energy is expressed as follows:

$$E_C^{\alpha\beta} = \int e_{\alpha\beta}^{UEG}\left[g_{\alpha\beta}(x_\alpha, x_\beta) + h_{\alpha\beta}(x_{\alpha\beta}, z_{\alpha\beta})\right]\mathrm{dr} \qquad \textbf{(2.34)}$$

where $g_{\alpha\beta}(x_\alpha, x_\beta)$ is;

$$g_{\alpha\beta}(x_\alpha, x_\beta) = \sum_{i=0}^{n} c_{C\alpha\beta,i}\left(\frac{\gamma_{C\alpha\beta}(x_\alpha^2 + x_\beta^2)}{1+\gamma_{C\alpha\beta}(x_\alpha^2 + x_\beta^2)}\right)^i \qquad \textbf{(2.35)}$$

and $h_{\alpha\beta}(x_{\alpha\beta}, z_{\alpha\beta})$ is expressed in Eq.2.27. Note that ${x_{\alpha\beta}}^2 \equiv x_\alpha^2 + x_\beta^2$ and $z_{\alpha\beta} \equiv z_\alpha + z_\beta$.

For parallel spins;

$$E_C^{\sigma\sigma} = \int e_{\sigma\sigma}^{UEG}[g_{\sigma\sigma}(x_\sigma) + h_{\sigma\sigma}(x_\sigma, z_\sigma)]D_\sigma dr \qquad \textbf{(2.36)}$$

where $g_{\sigma\sigma}(x_\sigma)$ is expressed as:

$$g_{\sigma\sigma}(x_\sigma) = \sum_{i=0}^{n} c_{C\sigma\sigma,i} \left(\frac{\gamma_{c\sigma\sigma} x_\sigma^2}{1+\gamma_{c\sigma\sigma} x_\sigma^2}\right)^i \quad \textbf{(2.37)}$$

and $h_{\sigma\sigma}(x_\sigma, z_\sigma)$ is defined in Eq. 2.27 D_σ is the self-interaction correction factor, which is:

$$D_\sigma = 1 - \frac{x_\sigma^2}{4(z_\sigma + C_F)} \quad \textbf{(2.38)}$$

D_σ disappers for one-electron systems. $e_{\alpha\beta}^{UEG}$ and $e_{\alpha\sigma}^{UEG}$ are the uniform electron gas (UEG) correlation energy density for the opposite-spin and parallel spin cases. Therefore, the M06-2X correlation energy is the sum of those;

$$E_C = E_C^{\alpha\beta} + E_C^{\alpha\alpha} + E_C^{\beta\beta} \quad \textbf{(2.39)}$$

In addition to those terms, $\gamma_{C\alpha\beta} = 0.0031$, $\gamma_{C\sigma\sigma} = 0.06$.

As stated before, M06-2X is a hybrid meta functional [48]. The hybrid exchange-correlation energy ($E_{XC}[\rho]$) can be defined as follows:

$$E_{XC}^{hyb} = \frac{X}{100} E_X^{HF} + \left(1 - \frac{X}{100}\right) E_X^{DFT} + E_C^{DFT} \quad \textbf{(2.40)}$$

where E_X^{HF} is the nonlocal Hartree-Fock (HF) exchange energy and the X is the percentage of HF exchange in the hybrid functional. This X value and other coefficients in these hybrid functionals are optimized to increase the accuracy of the functional to the given datasets [48]. The X value is evaluated “27” for the M06; therefore, the M06-2X functional includes 54% of E_X^{HF}.

The parameters of M06 functional is optimized with data sets including transition metals and non-metals; on the other hand, the M06-2X functional is parametrized only for non-metals. Thus, the M06-2X functional is recommended to study main-group thermochemistry, kinetics and noncovalent interactions. However, our benchmark calculations on ionization potentials of transition metals have shown that M06-2X gives better results than other common functionals.

2.3 ONIOM Extrapolated Scheme

Hybrid methods allow the combination of two or more computational techniques in one calculation and make it possible to investigate the chemistry of very large systems with high precision. In other words, the region of the system where the chemical process takes place, for example bond breaking or bond formation, is treated with an appropriately accurate method, while the remainder of the system is treated at a lower level. The most common class of hybrid methods is QM/MM systems that uses QM calculations for the high level system and MM calculations for the low level system. There is a variety of QM/MM hybrid energy methods in the literatures. ONIOM (our Own N-Layer Integrated molecular Orbital molecular Mechanics) is one of these schemes and has some advantages over others [43].

Three independent energy calculations are done to obtain the total energy of the system in a two-layered ONIOM system:

$$E^{\mathrm{ONIOM(QM:MM)}} = E_{model}^{QM} + E_{real}^{MM} - E_{model}^{MM} \qquad \textbf{(2.41)}$$

The real system contains all the atoms, and is calculated only at the MM level of the theory. The model system, on the other hand, contains only the atoms that are treated at the QM level. It also includes the link atoms that are used to cap dangling bonds resulting from cutting covalent bonds between the QM and the MM regions. In order to reduce the number of iteration steps and the computational cost, standard microiterations are implemented in ONIOM as default.

The electrostatic interactions between the layers are taken into account in two ways. In the simplest form, the interaction between the QM and MM region is completely described by molecular mechanic terms. The electrostatic interaction is evaluated as the interaction of the MM partial charges with point charges assigned to the atoms in the QM region. This approach is called as the classical/mechanical embedding (ME). The second approach is referred as charge/electronic embedding (EE). In this approach, the charge distribution of MM region interacts with the actual wave function of the QM region. The point charges from the MM region are included in the QM Hamiltonian, which allows the wave function to respond to the charge distribution of the MM region [44].

3. RESULTS AND DISCUSSION

3.1 Validation Of The Methodology

Fet3p is a ferroxidase protein, which has also cuprous oxidase activity. As stated before in section 2, the main reactions of Fet3p are oxidation-reduction reactions; therefore, the most crucial term is the ionization energy. If the ionization energies of the metals could be calculated correctly, the reaction energy calculations will be more reliable. In order to choose the best functional and basis set pair, a benchmark set has been formed. In this benchmark set, different functionals with various basis sets have been used to calculate the ionization energies of the transition metals.

The most common and used pure and hybrid DFT functionals have been tested as well as the other DFT functionals implemented in GAUSSIAN09. Different basis sets have been used with these functionals. The benchmark is listed in Table 3.1. The experimental molar IE's have been taken from Liao and Schneider's work [49].

A closer look at Table 3.1 reveals that, no method/basis set pair perform sufficiently well for all the transition metals considered. In order to calculate the reaction energies properly, different basis sets for different atoms with same method have been used. The results fall into two groups. One group includes only the copper atom. On the other hand, the second group has been formed by iron, cobalt and nickel. The best method, which calculates both groups IE accurately, has been found to be M06-2X. For copper the CEP-121G basis set has been selected, since it has calculated the Cu IE2 accurately, with 0,8 kcal/mol error. On the other hand, for the other group, the 6-31G basis set that calculates the IE's of these metals with minimal error, has been chosen.

The chosen functional, M06-2X has a high amount of (54%) Hartree-Fock exchange. As stated above in Section 2.2, it was optimized for only non-metals; thus Zhao and Truhlar recommended it for the metal-free systems [47]. However, the best result in the benchmark set has been obtained with the M06-2X functional. Therefore, M06-2X with the specified basis sets has been used in this study.

Table 3.1 : Ionization energies of transition metals with different method/basis sets (kcal/mol).

	Cu IE2	Co IE3	Fe IE3	Ni IE3
Experimental	**467.9**	**772.5**	**706.7**	**811.4**
B3LYP/6-31G	412.5	---	721.5	---
B3LYP/cc-PVDZ	476.1	---	729.5	---
BP86/6-31G	419.5	---	728.5	---
BP86/cc-PVDZ	484.9	---	735.7	---
BP86/CEP-121G	481.7	792.4	728.9	825
BP86/MDF10	484.2	796.4	734.6	833.8
BP86/MHF10	488.2	802.5	740.1	838.5
G96LYP/6-31G	416.5	---	724.7	---
G96LYP/cc-PVDZ	482.1	---	731.9	---
M06/6-31G	420.9	772.4	704.2	830.5
M06/6-31G*	420.8	771.2	704.4	830.6
M06/cc-PVDZ	474.7	776.1	708.7	835
M06/CEP-121G	476.1	789.5	736.8	829.9
M06/LanL2DZ	474.7	772.6	715	817.3
M06/MDF10	477.5	774.1	721.1	815.8
M06/MHF10	480.3	780.7	726.5	820.1
M062X/6-31G	398.8	770.7	711.2	809.6
M062X/6-31G*	398.5	770.8	711.5	808.2
M062X/CEP-121G	467.9	777.9	717.3	819.1
M062X/LanL2DZ	474.7	791.6	---	835.4
M062X/MDF10	473.2	779.6	720.3	824.9
M062X/MHF10	478	785.7	725.9	829.8
M06HF/6-31G	391.8	---	723.1	---
M06HF/cc-PVDZ	448.2	---	729.6	---
M06L/6-31G	407.0	777.3	706.9	822.1
M06L/CEP-121G	455.5	783.8	718.4	804.2
M06L/LanL2DZ	465.3	791.8	729.5	812.3
M06L/MDF10	466.1	780.8	717.5	802.7
M06L/MHF10	469.1	786.8	722.8	807.6
MOHLYP/6-31G	408.2	770.2	709.2	806.4
MOHLYP/cc-PVDZ	476.2	782.9	720.3	823.6
MOHLYP2/6-31G	406.6	759.9	696.9	796.7

Table 3.1 (Continued): Ionization energies of transition metals with different method/basis sets (kcal/mol).

MOHLYP2/cc-PVDZ	465.0	772.5	708.3	813.4
MPWLYP/6-31G	421.3	---	724.7	---
MPWLYP/cc-PVDZ	484.9	---	734.7	---
MPWLYP1M/6-31G	418.2	---	722.9	---
MPWLYP1M/cc-PVDZ	481.8	---	732.6	---
MPWLYP1W/6-31G	422.4	---	726.7	---
MPWLYP1W/cc-PVDZ	486.2	---	736.5	---
O3LYP/6-31G	417.6	---	716.4	---
O3LYP/cc-PVDZ	479.2	---	725.3	---
OLYP/6-31G	422.8	---	716.9	---
OLYP/cc-PVDZ	483.5	---	727	---
PBE/CEP-121G	481.0	788.2	723.6	823.1
PBE/LanL2DZ	485.6	808.7	749.4	846.2
PBE/MDF10	---	793.3	730.1	832.4
PBE/MHF10	486.6	799.5	735.7	837.3
PBE1W/6-31G	420.9	---	726.8	---
PBE1W/cc-PVDZ	486.6	---	735.8	---
PBELYP1W/6-31G	424.1	---	730.3	---
PBELYP1W/cc-PVDZ	490.3	---	740.1	---
TPSS/CEP-121G	473.9	785.8	718.9	809.7
TPSS/LanL2DZ	477.3	806.6	740.8	832.5
TPSS/MDF10	---	777.9	724.5	818.3
TPSS/MHF10	479.6	796.9	730.3	823.1
TPSSLYP1W/6-31G	415.5	---	726.2	---
TPSSLYP1W/cc-PVDZ	479.2	---	---	---
X3LYP/6-31G	410.8	---	719.3	---
X3LYP/cc-PVDZ	474.2	---	727.5	---

3.2 Nomenclature And Descriptions

In this study, the geometries of the products and reactants have been optimized. Between these two structures (reduced and oxidized substrate and/or oxidized and reduced cofactor states), there are only small geometric changes. Importantly, these small changes have been enough to cause the redox reactions. Nevertheless, since these two states are very similar, only the geometries with reduced substrate are given in the figures for every protonation state, if not indicated otherwise. In addition to the figures, the important geometric parameters (in Å) have been given in the corresponding tables.

Moreover, the oxidation states of the metal atoms have been determined by their spin densities. Spin density shows the number of unpaired electrons on the atom. Therefore, for Cu^{+}, the spin density equals to 0, whereas it is 1 for Cu^{+2}. The spin density is 4 for Fe^{+2}, and 5 for Fe^{+3}. For the rest of the transition metals, the spin densities equal to 3 for Co^{+2}, 4 for Co^{+3}, 2 for Ni^{+2} and 3 for Ni^{+3}. In the case of isolated atoms, spin densities are integer values. However, in the presence of ligands, due to the charge transfer interactions, there are some deviations from these values. The tables of spin densities have been given aside from the tables of geometric features. The sign of the spin densities, shows the type of unpaired electron on the atoms ("+" for alfa, "-" for beta).

The nomenclature used in this study is as follows. The OH^{-} near the T3 site has been named as OHT3, while the OH^{-} near the T2 site has been called as OHT2. Also, copper ions have been distinguished with their types: T1, T2, T3a and T3b. On the other hand, the reactions occur at different protonation states. To indicate the protonation state, the substrate number and the redox state, first the protonation site, followed by the substrate number and the substrate redox state (R for reduced, O for oxidized) has been specified in the structure name. For example, the structure $OHT3Fe_{1,R}$ means that the OHT3 is protonated and the 1st substrate iron is in reduced (Fe^{+2}) form, whereas $O^{-2}Fe_{2,O}$ means, the O^{-2} is protonated and the 2nd iron is oxidized to Fe^{+3}. Moreover, if the "N" letter is added in front of a protonation site name, that means all protonation sites but the indicated one are protonated. For example, $NOHT2_{3,O}$ means the 3rd substrate is oxidized and the OHT3 and O^{-2} are fully protonated. Additionally, to indicate the state with four protonations and without any protonations, the abbreviation of "all protonated" (AP) and "no protonation" (NP) has been used like $APFe_{4,O}$ and $NPFe_{1,R}$.

3.3 Optimizations Of Geometries With The Actual Subtrate

Fet3p catalyzes 4 substrate oxidations, and 4 copper reductions occur by the electrons coming from the substrate oxidations. During these reactions, there are 4 protonations as well. In order to calculate the reaction energy, the energies of the optimized reactants and products have been calculated. To obtain the reactants and products, the optimizations of the structures have been carried out in two sequential steps. First, the substrate site and copper site have been optimized separately for the intended oxidation states. During the optimization of each site, the atoms of the other site have been defined at the MM level and their coordinates have been frozen. Then, these two geometries have been combined and the full system has been optimized.

The NI structure has been designed according to the work of Rulíšek et al. [27]. In this structure, all cofactor copper ions are in the oxidized form. The O^{-2} ion resides at the center of the tri-nuclear copper cluster. One OH^{-} (OHT2) is located near the T2 site whereas the other one (OHT3) is positioned at the T3 site of the TNC. As indicated above, 4 protonations occur during the reactions. The protonations sites are OHT2, OHT3 and O^{-2} (the latter can take up to two protons).

3.3.1. Reactions with no protonation

In this first reaction, the situation where the iron oxidation occurs before any protonations has been modeled. Both the reactant $NPFe_{1,R}$ and the product $NPFe_{1,O}$ structures have been optimized. T1 has been reduced to Cu^{+} by the Fe^{+2} to Fe^{+3} oxidation. The reactant geometry is shown in Figure 3.1, and the geometric parameters and the spin densities of corresponding atoms are given in Table 3.2 and 3.3, respectively.

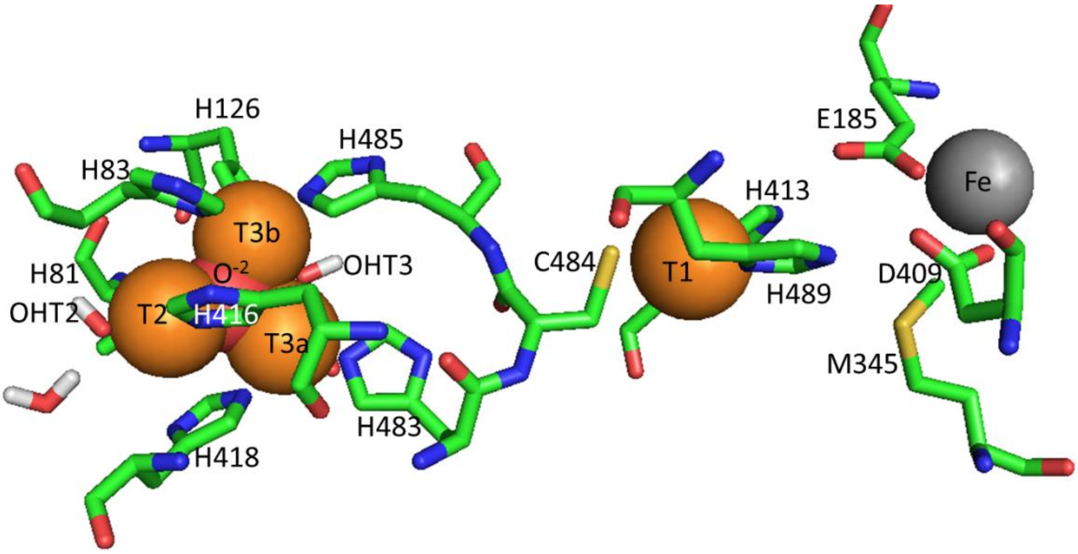

Figure 3.1 : The $NPFe_{1,R}$ geometry (Green sticks show carbon atoms, while red sticks/spheres stands for the oxygen atoms, grey sticks for hydrogen atoms, navy sticks for the nitrogen atoms, grey sphere for iron ion and orange spheres for the copper ions).

Table 3.2 : Important distances in Å for $NPFe_{1,R}$ and $NPFe_{1,O}$.

Residues	**$NPFe_{1,R}$**	**$NPFe_{1,O}$**
Fe - T1	8.173	8.388
Fe - D409	2.153	1.961
Fe - E185	1.996	1.850
Fe - M345	4.545	4.480
D409 - H413	1.576	1.768
E185 - H489	1.732	2.638
T1 - C484	2.239	2.347
T1 - H413	1.934	2.054
T1 - H489	1.938	2.078
T3a - T3b	2.968	2.964
T3a - T2	3.427	3.425
T3a - O^{-2}	1.934	1.940
T3a - OHT3	1.978	1.980
T3a - H128	2.375	2.384
T3a - H483	2.065	2.053
T3a - H418	2.090	2.091
T3b - T2	3.378	3.378
T3b - O^{-2}	1.930	1.930
T3b - OHT3	2.018	2.017
T3b - H83	2.122	2.126
T3b - H126	2.267	2.276
T3b - H485	2.093	2.085
T2 - O^{-2}	1.875	1.874
T2 - OHT2	1.974	1.978
T2 - H416	2.028	2.025
T2 - H81	2.042	2.045

Table 3.3: The spin densities of metallic atoms in $NPFe_{1,R}$ and $NPFe_{1,O}$ with antiferromagnetic coupling (AC) and ferromagnetic coupling (FC).

Atoms	**$NPFe_{1,R}$ (AC)**	**$NPFe_{1,O}$ (AC)**	**$NPFe_{1,R}$ (FC)**	**$NPFe_{1,O}$ (FC)**
T1	0.6575	0.0000	0.6575	0.0000
T3a	0.7089	0.7085	0.7154	0.7160
T3b	0.6888	0.6877	0.7066	0.7052
T2	-0.6659	-0.6648	0.6830	0.6829
Fe	3.8883	4.4751	3.8883	4.4750

Beside the antiferromagnetic structure (AF), the ferromagnetic structures (FC) have been optimized. The spin density table 3.3 shows both results. However, the geometries of AC and FC structures are exactly the same (the most significant difference between two corresponding structures are in ~0.001Å level); therefore, in Table 3.2 only the AC geometries are given.

As seen from Table 3.3, in both AC and FC states, the spin densities of T1 and iron change during this reaction from 0.66 to 0 and from 3.89 to 4.48, respectively. In other words, an electron from Fe^{+2} is transferred to T1 and T1 is reduced to +1 state. The energies of FC reactant and product are higher than AC ones by 0.4 kcal/mol, hence the transformation between two spin states is energetically possible. The reaction energy (ΔE) is calculated as +6.5 kcal/mol for both AC and FC states. The result suggests that although the reaction is endothermic, ΔE is low enough for the reaction to occur. However, to check the results, the reactant and product geometries have been re-optimized with electronic embedding from the optimized geometries with mechanical embedding (ME). The electronic embedding (EE) calculations are much more reliable. The reaction energy in the electronic embedding calculations turns out to be +27.1 kcal/mol. The electronic embedding result shows that the reaction is too endothermic to happen; thus, the reaction is not considered to occur without any protonations.

For the rest of the structures, only the mechanic embedding optimizations have been done yet and only ME results are given, because electronic embedding calculations are computationally expensive. Yet, it must be kept in mind, that ME underestimates the reaction energies significantly.

Although the reaction is unlikely to occur without protonation, the geometric features of the $NPFe_{1,R}$ and $NPFe_{1,O}$ are detailed here as a reference point to compare with the protonated states. The most significant changes happen at the sites where the redox reaction occurs. In Table 3.2, after Fe^{+2} to Fe^{+3} oxidation and T1 reduction to +1, iron moves towards the exit of the substrate-binding site and moves away by 0.2Å from T1. In addition, iron gets closer to E185 and D409 0.15Å and 0.19Å, respectively. The spin densities of E185 and D409 increase from 0.02 to 0.18 and from 0.01 to 0.1 respectively; thus, the charge transfer interactions of these residues with Fe^{+3} increase. The charge transfer interactions at the iron site and the T1 site are coupled through D409-H413 and E185-H489 interactions. Because of the increasing charge transfer interactions with the oxidized iron, E185 and D409 move away from their His ligands, by 0.9Å and 0.19Å. The hydrogen bond between D409 and H413 gets weaker whereas the hydrogen bond interaction between E185 and H489 disappears completely. Therefore, these changes make His residues a weaker electron donor and reduce the charge transfer interaction between His residues and T1; hence favor the reduced state of T1. Similarly, the reduced state of iron favors the oxidized state of copper.

Spectroscopic studies show that there is a highly covalent interaction between C484 and T1 [29]. Because $T1^{+2}$ is reduced to $T1^{+}$, it moves 0,1Å away from its ligand C484. This result is in agreement with the experimental data and this movement reduces the covalent interaction and the charge transfer interaction between two atoms. Furthermore, T1 moves away from its His ligands by ~0.13Å. Thus, the charge transfer interactions between the nitrogen atoms and T1 decrease. These interactions also contribute to the T1 redox potential, but not as importantly as the C484-T1 interaction does. On the other hand, the residues and the ions at the TNC site keep their initial positions during the reaction. In addition, the spin densities of the TNC coppers remain the same. These results suggest that TNC and T1 sites act uncoupled without any protonations.

Although it seems unlikely that the redox occur without any protonations, we have investigated the reaction of a second substrate. In order to represent this situation, an electron corresponding to the one left behind by the first substrate has been added to the system. For the $NPFe_{2,R}$ structure, the substrate-binding site has been optimized to a geometry in which iron is in the +2 state, whereas the copper site has been optimized to a geometry in which one copper is in the +1, and the remaining three coppers are in the +2 state. Then, these geometries have been combined and optimized again. Simultaneously, for the $NPFe_{2,O}$ structure, the substrate-binding site has been optimized such that iron is in +3 state, while the copper binding site has been optimized such that two coppers are in the +1 state and the other two coppers are in the +2 state. Again, these geometries have been combined and optimized.

In the trials to obtain the product state $NPFe_{1,O}$, no electron transfer has occurred from the iron to the coppers. Therefore, this state cannot be obtained and the optimizations have not been continued.

On the other side, two different structures have been obtained for the reactant structure, in which the additional electron comes and reduces either T1 or T3b. The spin densities are given in Table 3.4 for these structures.

Table 3.4 : The spin densities of metallic atoms in $NPFe_{2,R.}$

Atoms	$\mathbf{NP_IFe_{2,R}}$	$\mathbf{NP_{II}Fe_{2,R}}$
T1	0,0000	-0,6272
T3a	0,7086	0,6871
T3b	0,6879	-0,0030
T2	-0,6642	0,6640
Fe	3,8815	3,8878

The structure where T1 is reduced is named as $NP_IFe_{2,R}$ and, the structure with reduced T3b is named as $NP_{II}Fe_{2,R}$. The $NP_IFe_{2,R}$ structure gives the same spin densities with the $NPFe_{1,R}$ structure but the spin density of T1. The spin density of T1 diminishes due to the additional electron. On the other hand, in the $NP_{II}Fe_{2,R}$ structure, the T3b is reduced and there is no antiferromagnetic coupling in TNC. In addition, the spin density on the T1 is decreased by 0.03 in magnitude.

The structure $NP_IFe_{2,R}$ is energetically much more favorable. The energy difference between $NP_{II}Fe_{2,R}$ and $NP_IFe_{2,R}$ is +16.6 kcal/mol. The $NP_{II}Fe_{2,R}$ is higher in energy, therefore it appears that the replacement of the oxidized first substrate by a second substrate is not enough for the migration of the electron from T1 to TNC site. Hence, the migration of electron cannot be possible without any protonations.

The only geometric difference between $NP_IFe_{2,R}$ and $NPFe_{1,R}$ structures are seen at the T1 site to where the electron comes whereas the geometry of TNC remains the same (data not shown). The three ligands of the T1 move away from T1 and come to the positions they reside in $NPFe_{1,O}$ although in the latter structure iron is in the oxidized state. Therefore, the charge transfer interaction between these residues and the T1 is reduced. Here, the coupling between the iron site and the T1 site acts in two opposite directions. As a result of the reduction in charge transfer interactions between T1 and its histidine ligands tends to weaken the hydrogen bonds between these histidines and E185 and D409. This, in turn, tends to increase charge transfer between these residues and iron, favoring the oxidized state of this ion. On the other hand, the charge transfer interactions of E185 and D409 with Fe^{+2} are relatively weaker. Therefore, these residues tend to make stronger hydrogen bonds with histidines which would make them better electron donors. This would favor the oxidized state of copper by pushing an electron to TNC. As a result of these opposing effects, an intermediate geometry is formed. E185 and D409 move away from their His ligands by 0.20Å and 0.12Å, respectively, compared to $NPFe_{1,R}$. However these changes smaller than the changes in the oxidized state $NPFe_{1,O.}$ It appears that the coupling between the iron site and the T1 site is not strong enough to transfer an electron from Fe^{+2} or T1 to TNC. Nevertheless, its effects on the geometry suggest that it may contribute to the oxidation of these ions upon protonation.

In the case of $NP_{II}Fe_{2,R}$, the geometry of the substrate-binding site and the T1 site remain the same as in the $NPFe_{1,R}$ structure. However, this time, the geometry of the TNC site changes due to the additional electron. T2 and its ligands keep their positions. Due to the charge change of T3b, OHT3 rotates and orients its oxygen away from T3b. And also T3b moves from its position and get closer to T2 by 0.19Å and most significantly the distance of T3b and OHT3 increase by 1.15Å. Due to this changes the His128-T3a distance increase by 0.29Å.

3.3.2. Reactions with one protonation

As mentioned in the section 3.3.1., the reaction of first substrate is highly endothermic whereas the second substrate oxidation in those conditions is impossible. Thus, one proton is added to the system. As stated before, in NI state, there are three protonation sites: OHT2, OHT3 and O^{-2}. Therefore, one proton was added to each of these sites separately, and for each structure, the reactant and product structures have been optimized.

The redox product in the case of the protonated OHT2 ($OHT2Fe_{1,O}$) cannot be obtained; thus, it will not be discussed here. Thus, only the results of protonated OHT3 and O^{-2} structures are given at this point. The protonation of OHT3 yields a water molecule while the protonation of O^{-2} yields an OH^{-} ion. The reactant geometries are shown in Figure 3.2 and Figure 3.3, and the geometric parameters and the spin densities of corresponding atoms are given in Table 3.5 and 3.6, respectively.

Table 3.5 : Important distances in Å in singly protonated structures.

Residues	**OHT3Fe$_{1,R}$**	**OHT3Fe$_{1,O}$**	**O^{-2}Fe$_{1,R}$**	**O^{-2}Fe$_{1,O}$**
Fe - T1	8.185	8.439	8.162	8.392
Fe - D409	2.150	1.960	2.150	1.961
Fe - E185	2.004	1.853	2.002	1.853
Fe - M345	4.544	4.486	4.552	4.488
D409 - H413	1.547	1.757	1.549	1.759
E185 - H489	1.691	2.249	1.708	2.312
T1 - C484	2.251	2.357	2.252	2.359
T1 - H413	1.927	2.047	1.927	2.045
T1 - H489	1.933	2.070	1.932	2.067
T3a - T3b	3.152	3.149	3.153	3.153
T3a - T2	3.382	3.379	3.569	3.570
T3a - O^{-2}	1.933	1.935	2.102	2.108
T3a - OHT3	2.157	2.173	1.954	1.956
T3a - H128	2.190	2.188	2.254	2.262
T3a - H483	2.039	2.024	2.010	2.000
T3a - H418	2.114	2.119	2.056	2.056
T3b - T2	3.256	3.257	3.436	3.440
T3b - O^{-2}	1.898	1.898	2.052	2.052
T3b - OHT3	2.510	2.515	1.998	1.993
T3b - H83	2.097	2.105	2.094	2.100
T3b - H126	2.132	2.134	2.206	2.212
T3b - H485	2.057	2.045	2.029	2.022
T2 - O^{-2}	1.934	1.932	1.966	1.964
T2 - OHT2	1.974	1.979	1.940	1.942
T2 - H416	2.014	2.011	1.995	1.994
T2 - H81	2.033	2.034	2.043	2.043

Table: 3.6 : The spin densities of metallic atoms in OHT3Fe$_1$ and O^{-2}Fe$_1$.

Atoms	**OHT3Fe$_{1,R}$**	**OHT3Fe$_{1,O}$**	**O^{-2}Fe$_{1,R}$**	**O^{-2}Fe$_{1,O}$**
T1	0.6770	0.0000	-0.6775	0.0000
T3a	0.7536	0.7540	0.7288	0.7375
T3b	-0.7415	-0.7408	0.7508	0.7409
T2	0.6639	0.6630	0.6759	-0.6744
Fe	3.8751	4.4820	3.8867	4.4815

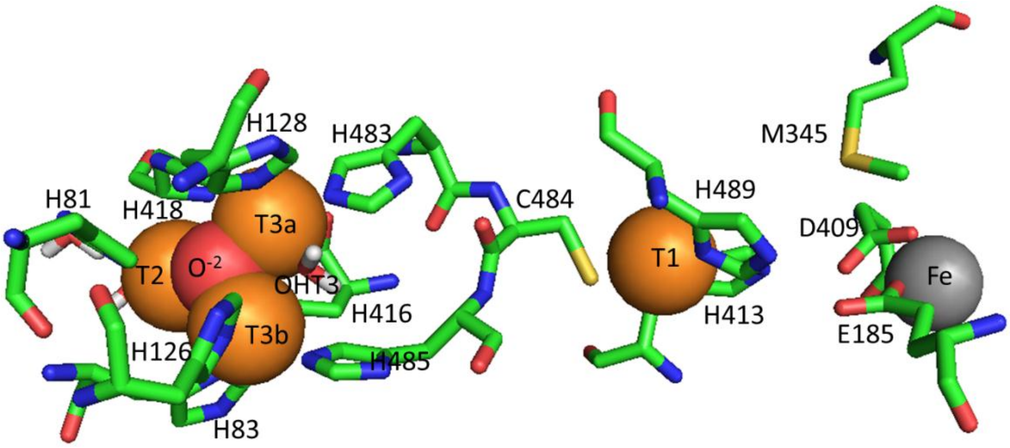

Figure 3.2 : The OHT3$Fe_{1,R}$ geometry (Green sticks show carbon atoms, while red sticks/spheres stands for the oxygen atoms, grey sticks for hydrogen atoms, navy sticks for the nitrogen atoms, grey sphere for iron ion and orange spheres for the copper ions).

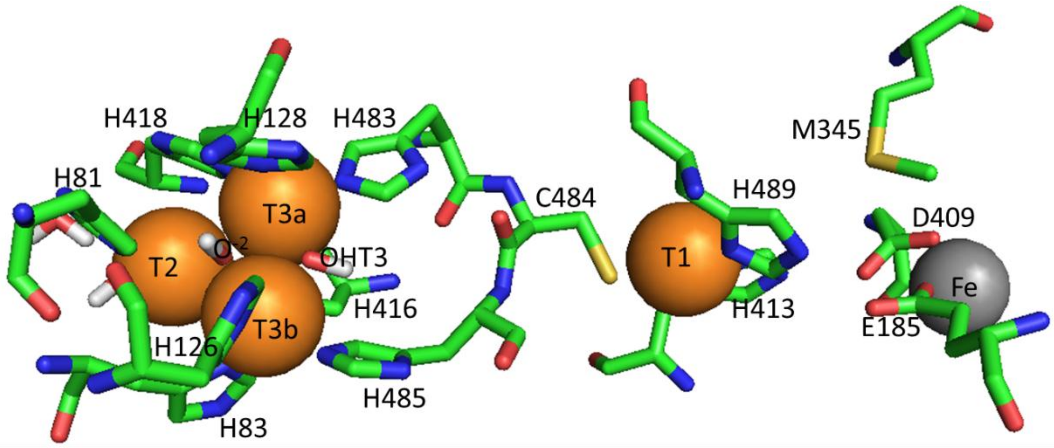

Figure 3.3 : The $O^{-2}Fe_{1,R}$ geometry (Color code is the same as the previous figure).

The reaction energies in the OHT3 protonated and O^{-2} protonated systems are -2,7 kcal/mol and -3,6 kcal/mol, respectively. In addition, the reactant and product of $O^{-2}Fe_{1,R}$ and $O^{-2}Fe_{1,O}$ are lower in energy than OHT3$Fe_{1,R}$ and OHT3$Fe_{1,O}$ by 3,7 kcal/mol and 5 kcal/mol respectively. Still both reactions are exothermic and energetically favorable. The reaction probably proceeds through $O^{-2}Fe_{1,R}$ since the reaction is more exothermic and $O^{-2}Fe_{1,R}$ is lower in energy than $OHT3_{1,R}$. Yet again, both structures are detailed below. On the other hand, when single point electronic embedding calculations have been done on the geometries optimized with mechanical embedding, the reaction of $O^{-2}Fe_{1,R}$ turns out to be endothermic by 17.2 kcal/mol, suggesting that the reaction in a singly protonated system is difficult and the product must be stabilized by a second proton. Nevertheless, electronic embedding optimizations are needed for more accurate results.

As seen from Table 3.6, after protonation of both sites, T1 is reduced by the electron coming from iron oxidation. The protonation of OHT3 affects the antiferromagnetism at the TNC site. The antiferromagnetism in the NI state, is found between T2 and T3 ions in $NPFe_{1,R}$ and $NPFe_{1,O}$. However, in the OHT3 protonated structures, the antiferromagnetism is observed between T3b and T3a/T2 (both ions have the same sign), as it is experimentally observed [27,31]. On the other hand, in the O^{-2} protonated structures the copper with the beta spin changes between the reactant and the product. However, this is not important and does not affect the reliability of the calculations, because the energy contribution of the direction of the spin is small as seen in the AC/FC structures above. Besides, the proton affects the spin density of T1. After protonation, the magnitude of the spin density of T1 increased from 0.66 to 0.68. This increase improves the redox potential of T1. The reduction in the reaction energy with respect to the non-protonated system can be due to this fact.

In the $OHT3F_{1,R}$ structure, OHT3 is protonated and forms a water molecule. This water molecule moves away from TNC. It goes 0.18Å and 0.50Å away from T3a and T3b, respectively. Due to this water formation, the charge transfer interactions of OHT3 (now water) and T3 coppers decrease. Therefore, the charge transfer interactions between T3 coppers and His ligands increase especially the ones with His ligands in H-C-H motif. Those changes cause a reduction in the electron donation capability of C484, thus; the charge interaction between T1 and C484 decreases. Hence, this situation increases the redox potential of T1 and facilitates the reduction of T1.

On the other hand, in $O^{-2}Fe_{1,R,}$ protonation converts O^{-2} ion to OH^{-} ion. The O^{-2} ion resides the middle of the tri-nuclear copper cluster and protonation of this ion decreases its charge, and therefore, reduces the interactions between oxygen atom and the positively charged (+2) copper atoms. Thus, the newly formed OH^{-} ion moves away from the copper atoms (0,1Å-0,15Å) and copper atoms moves away from each other due to the columbic repulsion. In this system too, T3 coppers attract electrons from histidines, a fact that reduces charge transfer from C484 to T1, facilitating the reduction of the latter. When the beta electron on T1 in $O^{-2}Fe_{1,R}$ or on T2 in $O^{-2}Fe_{1,O}$ is replaced by an alpha electron the energies remain the same, suggesting that antiferromagnetic coupling does not occur in these structures and there is no spin coupling between the T1 and TNC sites.

Apart from the ones stated above, the geometric parameters are the same as the structures in the non-protonated system during the redox event. In other words, the rest of the geometry of $OHT3Fe_{1,R}$ and $O^{-2}Fe_{1,R}$ are the same with the $NPFe_{1,R}$, and the geometries of $OHT3Fe_{1,O}$ and $O^{-2}Fe_{1,O}$ are the same with $NPFe_{1,O}$.

The reactions are exothermic after the protonations. As a further step, the second substrate oxidation has been tried to obtain with one protonation. The protonation may provide the necessary environment for second substrate oxidation. In order to do that, an electron has been added to the system.

Only the protonated OHT3 results for second substrate oxidation have been finished yet. However, the product $OHT3Fe_{2,O}$ cannot be obtained and the attempts for the product state optimization have given the reactant state. It is assumed that the second substrate oxidation cannot happen without the second protonation. In the reactant state, T3b is in +1 state (the corresponding data not shown in table). The state, where T1 is in +1, has not been sought too much. Therefore, the energies of two states cannot be compared. Yet, the protonation and the presence of the second substrate might favor the electron migration from T1 to T3b and stabilize T3b in the +1 state.

3.3.3. Reactions with two protonations

The second protonation yields four different structures. Those structures are as follows: one protonation to each of OHT2 and OHT3, one protonation to each of OHT2 and O^{-2}, one protonation to each of OHT3 and O^{-2}, and two protonations to O^{-2}. However, the geometry optimizations of these structures are still running, therefore; these results will be given in a future report.

3.3.4. Reactions with three protonations

The third protonation yields three different structures. There is only protonation site left in each of those structures and thus they are named according to their remaining protonation site. The structures are as follows: the one in which the OHT2 is still not protonated, the one in which the OHT3 is still not protonated, and the one in which

O^{-2} is only protonated once. The reactant and product geometries have been optimized. In the structure $NOHT3Fe_{3,O}$, a proton from O^{-2} is transferred to the OHT3; thus, this attempt also yielded into the $NO^{-2}Fe_{3,O.}$ The structure $NOHT3Fe_{3,O}$ is not discussed here. The reactant geometries of $NO^{-2}Fe_{3,R}$ and $NOHT2Fe_{3,R}$ is shown in Figure 3.4 and 3.5, respectively; and the geometric parameters and the spin densities of corresponding atoms are given in Table 3.7 and 3.8.

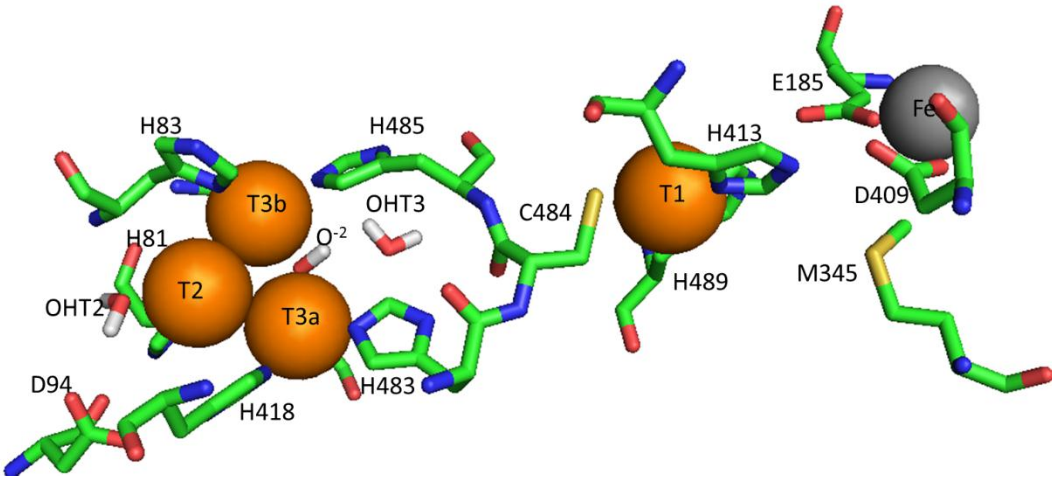

Figure 3.4 : The $NO^{-2}Fe_{3,R}$ geometry (Green sticks show carbon atoms, while red sticks/spheres stands for the oxygen atoms, grey sticks for hydrogen atoms, navy sticks for the nitrogen atoms, grey sphere for iron ion and orange spheres for the copper ions).

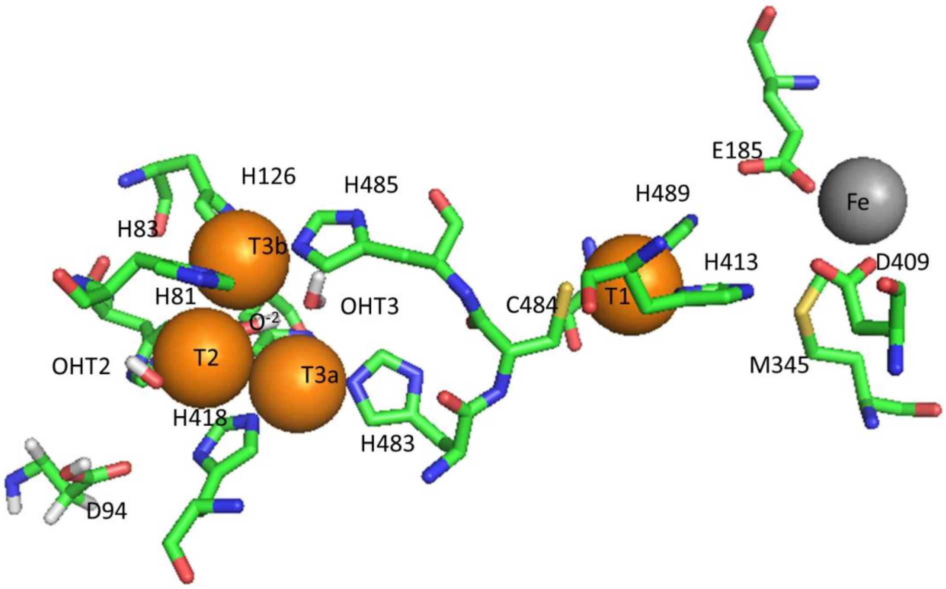

Figure 3.5 : The $NOHT2Fe_{3,R}$ geometry (Color code is the same as the previous figure).

Table 3.7 : Important distances in Å in thirdly protonated structures.

Residues	NO^{-2} $Fe_{3,R}$	NO^{-2}_{I} $Fe_{3,O}$	NO^{-2}_{II} $Fe_{3,O}$	NOHT2 $Fe_{3,R}$	NOHT2 $Fe_{3,O}$
Fe - T1	8.173	8.399	8.326167	8.146	8.313
Fe - D409	2.151	1.961	1.961	2.150	1.960
Fe - E185	1.999	1.851	1.861	2.002	1.864
Fe - M345	4.534	4.477	4.488	4.544	4.498
D409 - H413	1.558	1.761	1.716	1.555	1.715
E185 - H489	1.709	2.328	2.010	1.718	2.005
T1 - C484	2.244	2.352	2.214	2.247	2.221
T1 - H413	1.931	2.051	1.950	1.928	1.944
T1 - H489	1.934	2.068	1.954	1.934	1.952
T3a - T3b	3.830	3.840	3.959	4.869	4.356
T3a - T2	3.373	3.367	3.572	3.771	3.891
T3a - O-2	1.874	1.876	2.108	2.662	2.277
T3a - OHT3	4.304	4.321	3.395	2.816	3.655
T3a - H128	2.089	2.090	2.366	2.116	2.255
T3a - H483	2.051	2.038	2.045	1.973	2.004
T3a - H418	1.977	1.978	2.050	2.007	2.005
T3b - T2	3.542	3.538	3.468	3.505	3.556
T3b - O-2	2.199	2.194	2.154	2.506	2.297
T3b - OHT3	4.467	4.491	3.554	3.219	3.699
T3b - H83	2.051	2.052	2.088	2.039	2.035
T3b - H126	2.072	2.073	2.157	2.037	2.105
T3b - H485	2.235	2.226	2.171	2.115	2.142
T2 - O-2	3.546	3.518	3.396	2.060	3.345
T2 - OHT2	2.318	2.327	2.391	1.970	2.140
T2 - H416	1.971	1.969	1.972	1.954	1.978
T2 - H81	1.981	1.981	1.982	2.023	2.021

Table: 3.8 : The spin densities of metallic atoms in thirdly protonated structures

Atoms	NO^{-2} $Fe_{3,R}$	NO^{-2}_{I} $Fe_{3,O}$	NO^{-2}_{II} $Fe_{3,O}$	NOHT2 $Fe_{3,R}$	NOHT2 $Fe_{3,O}$
T1	0.6731	0.0000	0.5975	0.6734	0.6093
T3a	0.6911	0.6909	0.0000	0.0016	0.0000
T3b	0.0063	0.0067	0.0000	0.0016	0.0000
T2	0.0117	0.0116	0.0000	0.6621	0.0000
Fe	3.8747	4.4807	4.4887	3.8762	4.4895

As seen from Table 3.8, there are two different structures for $NO^{-2}Fe_{3,O}$: one with T1 in the +2 state and one with T3a in +2 and the remaining coppers in the +1 state. The reaction energy of the $NO^{-2}Fe_{3,R}$ to $NO^{-2}{}_{I}Fe_{3,O}$ where the T3a is in +2 state, is calculated as +4.0 kcal/mol. The other reaction energy where only the T1 is in +2 state in the product, is calculated more endothermically +16.0 kcal/mol. On the other hand, the reaction energy for the structures where all protonation sites except the OHT2 are protonated is calculated exothermically -14.5 kcal/mol.

Apart from the difference in protonation sites, the main geometric difference between two reactant geometries is that in the $NO^{-2}Fe_{3,R,}$ one newly formed water molecule (from OHT3) moves to the solvent channel near T3 site and the protonated O^{-2} takes the old place of OHT3, whereas in the $NOHT2_{3,R}$ they remain at their initial positions.

In the $NO^{-2}{}_{I}Fe_{3,O,}$ only the T3a copper is in the +2 state and other three coppers are in the +1 state; thus, protonated O^{-2} is near the T3a and shields the electrostatic repulsion of positively charged coppers. Due to the blockage of the protonated O^{-2}, the protonated OHT3 moves out to the water channel near the T3 site.

On the other hand, in the $NO^{-2}{}_{II}Fe_{3,O,}$ the negative charge of the protonated O^{-2} is shared with the protonated OHT3 and therefore cannot shield the electrostatic repulsion. Thus, in order to balance the electrostatic repulsion between coppers, the T2 and T3 coppers are in the +1 state and T1 is in the +2 state.

In the $NOHT2Fe_{3,R,}$ the T1 and T2 is in +2 and T3s are in the +1 state. The doubly protonated O^{-2} is positioned near the T2 and allows the protonated OHT3 to be positioned at the mid of the T3s. Therefore, the electron from the substrate oxidation comes directly to the T2 copper.

The numbers of atoms in these two systems are different; therefore, their energies cannot be compared. Yet, the numbers of atoms of the QM region are the same and so the energies of two systems of QM region can be compared. Due to the protonation site differences, there is a 8 kcal/mol energy difference between two optimized reactant QM regions ($NOHT2_{3,R}$ and $NO^{-2}Fe_{3,R}$). The $NOHT2_{3,R}$ is more stable. Since the $NOHT2_{3,R}$ is energetically more stable and the reaction energy is more favorable, the reaction probably proceeds through $NOHT2_{3,R}$.

3.3.5. Reactions with four protonations

The fourth protonation yields only one structure in which all of the protonation sites are protonated. The reactant $APFe_{4,R}$ and product $APFe_{4,O}$ have been optimized. The reactant geometry is shown in Figure 3.6, and the geometric parameters and the spin densities of corresponding atoms are given in Table 3.9 and 3.10, respectively.

Table 3.9 : Important distances in Å for $APFe_{4,R}$ and $APFe_{4,O}$.

Residues	**$APFe_{4,R}$**	**$APFe_{4,O}$**
Fe - T1	8.151	8.372
Fe - D409	2.153	1.961
Fe - E185	1.998	1.851
Fe - M345	4.539	4.475
D409 - H413	1.562	1.761
E185 - H489	1.722	2.418
T1 - C484	2.239	2.349
T1 - H413	1.930	2.050
T1 - H489	1.935	2.070
T3a - T3b	4.345	4.339
T3a - T2	3.787	3.772
T3a - H128	2.240	2.247
T3a - H483	2.004	1.997
T3a - H418	2.004	2.003
T3b - T2	3.668	3.653
T3b - OHT3	3.679	3.682
T3b - H83	2.033	2.037
T3b - H126	2.104	2.111
T3b - H485	2.148	2.141
T2 - OHT2	2.317	2.329
T2 - H416	1.970	1.967
T2 - H81	1.995	1.993

Table 3.10 : The spin densities of metallic atoms in $APFe_{4,R}$ and $APFe_{4,O}$.

Atoms	**$APFe_{4,R}$**	**$APFe_{4,O}$**
T1	0.6671	0.0000
T3a	0.0000	0.0000
T3b	0.0000	0.0000
T2	0.0000	0.0000
Fe	3.8888	4.4799

As it seen from table 3.10, the spin density of T1 is 0.67 in $APFe_{4,R}$ and 0 in $APFe_{4,O}$. The reaction energy is calculated as 5.2 kcal.

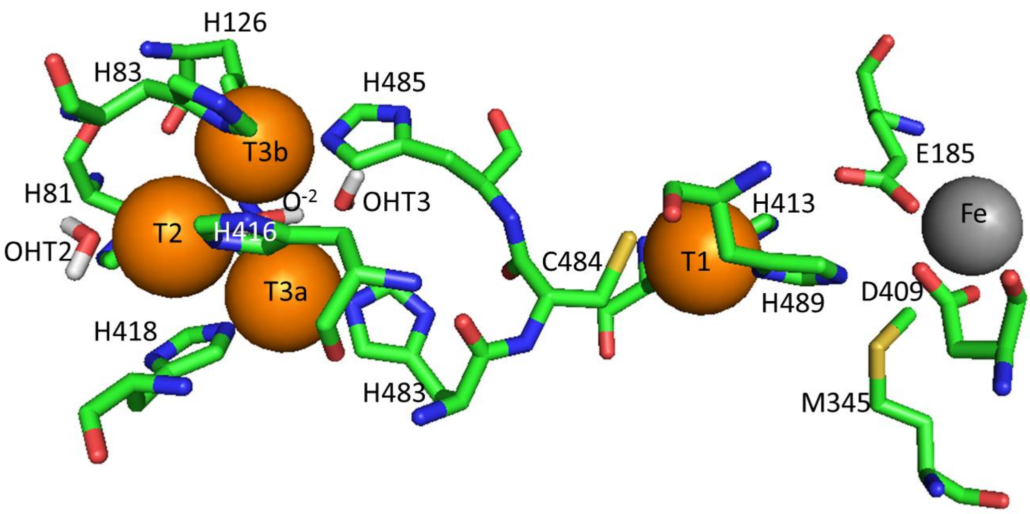

Figure 3.6 : The $APFe_{4,R}$ geometry (Color code is the same as the previous figure.)

As a consequence of four protonations, two water molecules are formed from OHT3 and O^{-2}. In Figure 3.4, it is seen that these two water molecules moves from their initial positions to the solvent channel near the T3 site and they start to leave the system in order to allow another dioxygen molecule to come and bind to the TNC.

The protonations on the other hand, removes the negative charges in the middle of the TNC and around the TNC. Therefore, the electronic repulsions between the copper ions increase, and they have a tendency to be in the +1 state. Also, the distances between the copper atoms increase.

On the other hand, one of the most significant displacement between the reactant and the product structures for every protonation states, has been occurred by iron. After substrate oxidation, Fe^{+3} moves 0,2Å away from T1 due to the increasing charge of the iron. The columbic repulsion between Fe^{+3} and the positively charged copper site directs the Fe^{+3} to the exit of the substrate-binding site and, hence, helps the transfer of iron to the Ftr1p which transports the iron into the cell.

3.4. Optimizations Of Geometries With The Potential Substrates: Cu^{+}, Co^{+2}, Ni^{+2}

In order to investigate the substrate specifity of Fet3p, Cu^{+}, Co^{+2} and Ni^{+2} ions have been treated as the potential substrates of the reaction. Fe^{+2} in $NPFe_{1,R}$ has been replaced by these transition metals. The reactants and products of the redox reactions have been searched.

3.4.1. The case of Cu^{+} as potential substrate

Fet3p has also a cuprous oxidase activity. In order to see the differences seen in the experiments, Fe^{+2} has been replaced with Cu^{+}, and the reactant and product of the reaction have been optimized without any protonations. The reactant geometry is shown in Figure 3.5, and the geometric parameters and the spin densities of corresponding atoms are given in Table 3.11 and 3.12, respectively.

As seen from Table 3.12, the substrate copper is oxidized, whereas T1 is reduced. Although the product geometry is close to the product geometry of iron without any protonations, in the reactant structure, the interactions of the substrate copper is different from those of the iron. The substrate copper is 2Å closer to the T1 and 1Å closer to the sulphur atom of M345 than in the case of iron. It was shown experimentally that when M345 is mutated to alanine, k_{ET} of the reaction with the copper decreased and K_m increased [19]. The effects of M345A mutation on binding and oxidation were not seen with the substrate iron. Thus, the mutation of M345A disrupts the interaction of copper with the sulphur of M345 and increases the K_m value. In addition, if the transition structure is similar to the reactant structure, there might be an interaction between copper and M345 which would reduce the activation energy. Hence, M345 mutation would decrease the ET rate.

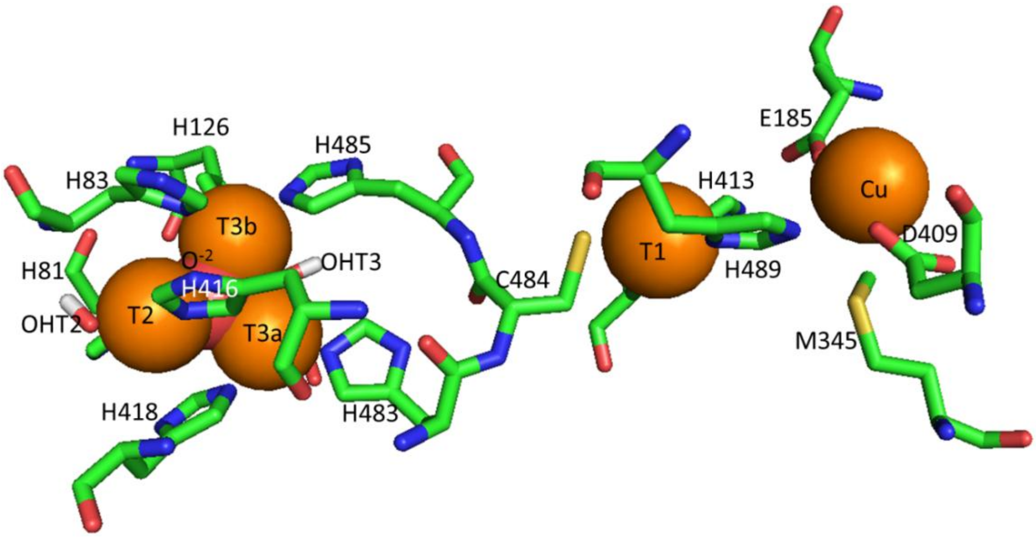

Figure 3.7 : The $NPCu_{1,R}$ geometry (Color code is the same as previous figures).

The reaction energy is calculated as 2,1 kcal/mol. The calculated reaction energy is lower than the related reaction energy with the iron substrate. This might be due to two reasons. First, the copper is oxidized from +1 to +2 state, whereas the iron is oxidized from +2 to +3 state. Therefore, the copper oxidation can happen more easily. The other reason is the interaction of the M345 with the substrate copper in the reactant structure, which is not seen with the substrate iron.

Table 3.11 : Important distances in Å for $NPCu_{1,R}$ and $NPCu_{1,O}$.

Residues	**$NPCu_{1,R}$**	**$NPCu_{1,O}$**
Cu - T1	6.255	8.366
Cu - D409	3.243	1.970
Cu - E185	2.016	2.059
Cu - M345	3.579	4.527
D409 - H413	1.665	1.694
E185 - H489	1.503	1.890
T1 - C484	2.266	2.361
T1 - H413	1.933	2.046
T1 - H489	1.931	2.058
T3a - T3b	2.969	2.962
T3a - T2	3.424	3.423
T3a - OHT3	1.980	1.980
T3a - H128	2.379	2.389
T3a - H483	2.061	2.048
T3a - H418	2.089	2.090
T3b - T2	3.376	3.379
T3b - OHT3	2.018	2.016
T3b - H83	2.119	2.129
T3b - H126	2.270	2.279
T3b - H485	2.094	2.080
T2 - OHT2	1.978	1.981
T2 - H416	2.027	2.025
T2 - H81	2.048	2.047

Table 3.12 : The spin densities of metallic atoms in $NPCu_{1,R}$ and $NPCu_{1,O}$.

Atoms	**$NPCu_{1,R}$**	**$NPCu_{1,O}$**
T1	-0.6882	0.0000
T3a	0.7150	0.7085
T3b	0.7068	0.6880
T2	0.6829	-0.6642
Cu	0.0000	0.8518

3.4.2. The case of Co^{+2} as potential substrate

In the case of cobalt as the potential substrate, like in the case of iron, the two parts of the active site – coppers site and the substrate-binding site- have been optimized separately to give the product geometry when combined. However, after combining the geometries of both sites, the optimizations result in the reactant geometry without any protonations and in the case of one protonation at OHT3 site. Since cobalt is a potential substrate for Fet3p, an extreme situation, low pH conditions, has been mimicked with four protonations. This situation maximizes the oxidizing power of Fet3p. Under these conditions, the reactions of the first substrate and the last substrate are studied. The spin densities of corresponding atoms for the geometries mentioned above are given in Table 3.13.

Table 3.13 : The spin densities of metallic atoms in $NPCo_1$, $OHT3Co_1$, $APCo_4$ and $APCo_1$.

Name	$NPCo_1$	$OHT3Co_1$	$APCo_4$	$APCo_1$
T1	0.6381	-0.6786	0.6570	0.6739
T3a	0.7081	0.7693	0.0000	0.8251
T3b	0.6869	0.7722	0.0000	0.8364
T2	-0.6653	0.6637	0.0000	-0.0013
Co	2.8320	2.8457	2.8355	3.3800

In the case of cobalt, a spin density slightly below 3 means that cobalt is in the +2 state, whereas a value slightly below 4 means that cobalt in the +3 state. As it seen from Table 3.13, the attempts to get the product geometry have been resulted in the reactant geometry for $NPCo_1$, $OHT3Co_1$ and $APCo_4$. The redox reactions cannot be happen for these structures. On the other hand, in an extreme condition, at low pH conditions, where all of the protonation sites are protonated, the first substrate Co^{+2} can be oxidized to Co^{+3}. Therefore, Fet3p can oxidize cobalt; yet, not as efficient as it oxidizes iron, because it cannot oxidize the last cobalt substrate.

3.4.3. The case of Ni^{+2} as potential substrate

In the case of nickel, to obtain the product structure $NPNi_{1,O}$, an attempt has been made to optimize the substrate-binding site in the presence of Ni^{+3}. However, this optimization has yielded Ni^{+2}, with nickel approaching E185 and taking an electron from it. In this calculation, copper ions are in the MM region. Nevertheless, considering the high tendency of nickel to be reduced, it is highly unlikely that the redox reaction, where an electron from the oxidation of nickel reduces a copper ion, takes place; or even if it happens, nickel will take an electron from its ligand E185 to be reduced back to Ni^{+2}.

4. CONCLUSIONS AND RECOMMENDATIONS

Fet3p is a membrane-bound yeast protein and responsible for the dioxygen reduction to water molecule by oxidizing 4 iron ions sequentially. Fet3p has four copper ions as cofactor and is a member of the multicopper oxidase family. In summary, the copper ions reduce a dioxygen molecule, and then by 4 Fe^{+2} oxidations, the copper ions are reduced and 4 H^{+} come from the environment and form 2 water molecules during the substrate oxidation reactions.

In order to investigate the substrate oxidation reactions, the potential reactants and products have been designed and optimized. By looking at the reaction energies, a potential substrate oxidation route is proposed.

The reaction energy is calculated as +6.4 kcal/mol without any protonations. The reaction energy for the second substrate cannot be calculated because the corresponding product geometry cannot be obtained. Then, a proton is added to the system. With an additional proton the reaction energies are calculated as -2.7 kcal /mol and -3.6 kcal/mol depending on the protonation site (OHT3 site and O^{-2} site respectively). The addition of a proton makes the endothermic reaction an exothermic one. It must be noted also that when the O^{-2} site is protonated the antiferromagnetic coupling within TNC disappears. This finding confirms that the native intermediate, where this coupling has been observed experimentally, corresponds to the non-protonated state as mentioned in the literature. The second substrate reaction energy cannot be calculated again because the product geometry cannot be obtained. The geometry optimization of second protonation with second substrate and third substrate are running still and therefore their results are unknown yet. Moreover, the reaction energy in triply protonated system with the third substrate is calculated as -14.5 kcal/mol for the structure where each of the three protonations site are protonated but the one at OHT2. The products of the other two structures are yielded to the same protonation structure where each three protonation sites are protonates once and their reaction energies are calculated endothermic 4.0

kcal/mol. In addition, when the all protonation site are protonated, the reaction energy for the 4th substrate oxidation is calculated as 5,2 kcal/mol.

Electronic embedding calculations on a few structures suggest that mechanical embedding calculations underestimate the reaction energies and the actual reaction energies are higher.

The following mechanism can be proposed: Because of the positive net charge (+2) at the TNC, protonations of all protonation sites are not expected to be at once, rather the protonations are expected to take place step by step. First, the protonation occurs then the substrate oxidation; transfer of an electron from the substrate to the copper site decreases the positive charge in the copper site and facilitates a new protonation. This protonation triggers the oxidation of the next substrate and so on. This cycle is repeated until all coppers are reduced. So the system returns to the fully reduced state and a new reaction can begin.

During these processes, two water molecules are formed from OHT3 and O^{-2}(which are formed from the dioxygen cleavage). In the state $APFe_{4,O,}$ the water molecules moves to the T3 site, in order to leave the system from the channel near the T3 site.

In addition, another result, which is in agreement with the experiments, is that the T1-Cys484 distance has a key role of the redox state of T1. The interaction between T1 and the sulphur atom of Cys484 is highly covalent. The charge transfer interactions between T1 and C484 and its other two ligands H413 and H489 affect the spin density of T1 or vice versa. When the charge transfer interactions between T1 and its ligands increase, the spin density of T1 reduces. This makes the taking of an electron by T1 harder. Therefore, the redox reaction becomes easier. This situation suggests that there is a direct relation between the reaction energy and the spin density of T1.

The substrate oxidation moves the oxidized substrate 0,2Å away from T1 due to the increasing charge of the iron and the columbic repulsion between oxidized iron and the positively charged copper site. Therefore the iron moves to the exit of the substrate-binding site assisting the transfer into the cell by Ftr1p.

In order to see the substrate specificity and detoxification mechanism of Fet3p, the Fe^{+2} in $NPFe_{1,R}$ has been replaced by Cu^{+}, Co^{+2} and Ni^{+2}.

Fet3p has cuprous oxidase activity also [18]; thus, the oxidation of Cu^{+} is expected. Without any protonation, the substrate Cu^{+} is oxidized to Cu^{+2} by Fet3p and the reaction energy is calculated as +2,1 kcal/mol. This reaction energy is lower than the iron oxidation energy without any protonation. This might be due to two possible reasons. In the reaction of iron, iron is oxidized from +2 to +3, whereas in the case of copper as substrate; copper is oxidized from +1 to +2. On the other hand, the interactions of Cu^{+} are different from the interactions of Fe^{+2}. Cu^{+} is 2Å more closer to T1 than Fe^{+2} and it is closer to Met345. The distance between substrate Cu^{+} and M345 decreases from 4,6Å to 3,6Å. If the transition state is close to the reactant geometry of Cu^{+} oxidation, the M345 might have a contribution to the reaction energy. Therefore, the reaction energy of the copper oxidation is calculated lower in energy than iron oxidation. This suggests that the upregulation of Fet3p under the copper stress conditions is due to detoxify the pro-oxidant form of Cu^{+} into less toxic form of Cu^{+2}.

In the case of Co^{+2}, cobalt cannot be oxidized without any protonations. An extreme scheme has been designed. In this extreme scheme, the reaction is modeled at a very low pH. When all protonation sites are protonated, the first substrate Co^{+2} can be oxidized to Co^{+3}. However, under the same conditions, the 4th Co^{+2} cannot be oxidized. This suggests that even if the cobalt is oxidized by Fet3p, the efficiency is lower than the efficiency with iron.

In the case of Ni^{+2}, nickel has a tendency to be in +2 state, thus; the oxidized state cannot be obtained. This suggests that in the Ni^{+2} stress conditions, the effect of Fet3p is to increase the iron uptake and not to oxidize Ni^{+2}

In future work, the geometries can be optimized with electronic embedding in order to get more reliable results. In addition, the D283A mutation has an increase in Km of iron, and D283 is in the MM region in these calculations because it is away from the substrate. Therefore, in order to see the effect of D283, this residue can be brought near the substrate-binding site, and then the optimization can be repeated. Besides, other mutations E185A and D409A can be designed and optimized and then results can be compared with the experimental results. For case of the substrate Cu^{+} and Co^{+2} the protonated structures can be optimized and the reaction energies can be calculated. These opinions can be the main subjects of the future studies.

REFERENCES

[1] **Liao, G., Liao D. and Li Q.** (2008). Heavy metals contamination characteristics in soil of different mining activity zones, *Transactions of Nonferrous Metals Society of China*, **18**, 207-211.

[2] **Wang, X., Liu L. and Jacobson A. J.** (2006). Synthesis and Structures of A Series of Novel Rare Earth Transition Metal Sulfates, *Journal of Rare Earths*, **24**, 656-662.

[3] **Cherian, M. G., and Nordberg M.** (1983). Cellular adaptation in metal toxicology and metallothionein, *Toxicology*, **28**, 1-15.

[4] **Donatan, S., Yazici, H., Bermek, H., Sarikaya, H., Tamerler, C., and Urgen M.** (2009). Physical elution in phage display selection of inorganic-binding peptides, *Materials Science and Engineering C*, **29**, 14-19.

[5] **Madureira N. L.** (2012). The iron industry energy transition, *Energy Policy*, **50**, 24-34.

[6] **Çakar, Z. P., Alkım, C., Turanlı, B., Tokman, N., Akman, S., Sarıkaya, M., Tamerler, C., Benbadis, L., and François J. M.** (2009). Isolation of cobalt hyper-resistant mutants of Saccharomyces cerevisiae by in vivo evolutionary engineering approach, *Journal of Biotechnology*, **143**, 130-138.

[7] **Maxim L . D.** (1989). Exchange rate developments and primary copper industry, *Resources Policy*, **15**, 156-168.

[8] **Bleackley, M. R., Young, B. P., Loewen, C. J. R. and MacGillivray R. T. A.** (2011). High density array screening to identify the genetic requirements for transition metal tolerance in Saccharomyces cerevisiae, *Metallomics*, **3**, 195-205.

[9] **Quintanar, L., Yoon, J., Aznar, C. P., Palmer, A. E., Andersson, K. K., Britt, D. R. and Solomon E. I.** (2005). Spectroscopic and electronic structure studies of the trinuclear Cu cluster active site of multicopper oxidase laccase: Nature of its coordination unsaturation, *Journal of American Chemical Society*, **127**, 13832-13845.

[10] **Tamilarasan, R. and McMillin, D. R.** (1989). Spectroscopic studies of the type 2 and type 3 copper centres in mercury derivative of laccase, *Biochem. J.*, **263**, 425-429.

[11] **Kupchak, B. R., Garitaonandia, I., Villa, N. Y., Mullen, M. B., Weaver, M. G., Regalla, L. M., Kendall, E. A. and Lyons T. J.** (2007). Probing the mechanism of FET3 repression by Izh2p overexpression, *Biochimica et Biophysica* Acta, **1773**, 1124-1132.

[12] **Metz, M. and Solomon, E. I.** (2001). Dioxygen binding to deoxyhemocyanin: Electronic structure and mechanism of the spin forbidden two electron reduction of O_2, *Journal of American Chemical Society*, **123**, 4938-4950.

[13] **Brändèn R., Malmström B. G. and Vänngård T.**. (1973). The effect of fluoride on the spectral and catalytic properties of three copper-containing oxidases, *Eur. J. Biochem.*, ***36***, 195-200.

[14] **Kwok, E. Y., Stoj, C. S., Severance, S. and Kosman, D. J.** (2006). An engineered bifunctional high affinity iron uptake protein in the yeast plamsa membrane, *Journal of Inorganic Biochemistry*, **100**, 1053-1060.

[15] **Lowery, M. D., Guckert, J. A., Gebhard, M. S. and Solomon E. I.** (1993). Active-site electronic structure contributions to electron transfer pathways in rubredoxin and plastocyanin: Direct versus superexchange, *Journal of American Chemical Society*, **115**, 3012-3013.

[16] **Silva D., Davis-Kaplan, S., Fergestad, J. and Kaplan J.** (1997). Purification and characterization of Fet3 protein, a yeast homologue of ceruloplasmin, *Journal of Biological Chemistry*, **272**, 14208-14213.

[17] **Ferraroni, M., Matera, I., Chernykh, A., Kolomytseva, M., Golovleva, L. A., Scozzafava, A. and Briganti F.** (2012). Reaction intermediates and redox state changes in a blue laccase from *Steccherinum ochraceum* observed by crystallographic high/low X-ray dose experiments, *Journal of Inorganic Biochemistry*, **111**, 203-209.

[18] **Stoj, C. and Kosman, D. J.** (2003). Cuprous oxidase activity of yeast Fet3p and human ceruloplasmin: implication for function, *FEBS Letters*, **554**, 422-426.

[19] **Stoj, C., Augustine, A. J., Solomon, E. I. and Kosman, D. J.** (2007). Structure-function analysis of the cuprous oxidase activity in Fet3p from *Saccharomyces cerevisiae, Journal of Biological Chemistry*, **282**, 7862-7068.

[20] **Shi, X., Stoj, C., Romeo, A., Kosman, D. J. and Zhu., Z.** (2003). Fre1p Cu^{2+} reduction and Fet3p Cu^{+} oxidation modulate copper toxicity in *Saccharomyces cerevisiae, Journal of Biological Chemistry*, **278**, 50309-50315.

[21] **Bleackley, M. R., Young, B. P., Loewen, C. J. R., and Mac Gillivray, R. T. A.** (2011). High density array screening to identify the genetic requirements for transition metal tolerance in *Saccharomyces cerevisiae*, *Metallomics*, **3**, 195-205.

[22] **Cakar, Z. P. et al.** Unpublished work**.**

[23] **Chaboy, J., Diaz-Moreno, S., Diaz-Moreno I., Rosa, M. and Diaz-Quintana A.** (2011). How the local geometry of the Cu-binding site determines the thermal stability of blue copper proteins, *Chemistry & Biology Chemistry*, **18**, 25-31.

[24] **Stoj, C., Augustine, A. J., Zeigler, L., Solomon, E. I. and Kosman, D. J.** (2006). Structural basis of the ferrous iron specificity of the yeast ferroxidase, Fet3p, *Biochemistry*, **45**, 12741-12749.

[25] **Solomon, E. I., Augustine, A. and Yoon, J.** (2008). O_2 reduction to H_2O by the multicopper oxidases, *Dalton Transactions*, 3921-3932.

[26] **Augustine, A. J., Kragh, M. E., Sarangi, R., Fujii, S., Liboiron, B. D., Stoj, C., and Kosman, D. J., Hodgson, K. O., Hedman, B., and Solomon, E. I.** (2008). Spectroscopic studies of perturbed T1 Cu sites in the multicopper oxidases *Saccharomyces cerevisiae* Fet3p and *Rhus vernicifera* Laccase: Allosteric Coupling between the T1 and trinuclear Cu sites, *Biochemistry*, **47**, 2036-2045.

[27] **Rulišek, L., Solomon, E. I. And Ryde U.** (2005). A combined quantum and molecular mechanical study of the O_2 reductive cleavage in the catalytic cycle of multicopper oxidases, *Inorganic Chemistry*, 44, 5612-5628.

[28] **Xu, F., Palmer, A. E., Yaver, D. S., Berka, R. M., Gambeta G. A., Brown, S. H. and Solomon, E. I.** (1999). Targeted mutations in a *Trametes villosa* Laccase, *Journal of Biological Chemistry*, **274**, 12372-12375.

[29] **Solomon, E. I.** (2006). Spectroscopic methods in bioinorganic chemistry :Blue to green red copper sites, *Inorganic Chemistry*, **45**, 8012-8025.

[30] **Patti, M. C. B., Felice M. R. Domenico, I. Lania, A., Alaleona, F. And Musci, G.** (2005). Spesific aspartate residues in FET3 control high-affinity iron transport in *Saccharomyces cerevisiae*, Yeast, **22**, 677-687.

[31] **Quintanar, L., Stoj, C., Taylor., A. B., Hart, P. J., Kosman, D. J. and Solomon, E. I.** (2007). Shall we dance? How a multicopper oxidase chooses its electron transfer partner, *Accounts of Chemical Research ReInorganic Chemistry*, **40**, 445-452.

[32] **Djoko, K. Y., Chong, L. X., Wedd, A. G. and Xiao, Z.** (2010). Reaction mechanism of multicopper oxidase CueO from *Escherichia coli* support its functional role as a cuprous oxidase, *Journal of American Chemical Society*, **132**, 2005-2015.

[33] **Taylor, A. B., Stoj, C. S., Ziegler, L., Kosman, D. J. and Hart, J.** (2005). The copper-iron connection in biology: Structure of the metallo-oxidase Fet3p, *PNAS*, **102**, 15459-15464.

[34] **Piontek, K., Antorini, M. and Choinowski, T.** (2002). Crystal structure of a laccase from the fungus *Trametes versicolor* at 1.90Å resolution containing a full complement of coppers, *Journal of Biological Chemistry*, **277**, 37663-37669.

[35] **Ferraroni, M., Myasoedova, N., M., Schmatchenko, V., Leontievsky, A. A., Golovleva, L. A., Scozzafava, A. and Briganti F.** (2007). Crystal structure of a blue laccase from *Lentinus tigrinus*:evidences for intermediates in the molecular oxygen reductive splitting by multicopper oxidases, *BMC Structural Biology*, **7**:60.

[36] **Yoon, J. and Solomon, E. I.** (2007). Electronic structure of the peroxy intermediate and its correlation to the native intermediate in the multicopper oxidases: Insights into the reductive cleavage of the O-O bond, *Journal of American Chemical Society*, **129**, 13127-13136.

[37] **Agustine, A. J., Quintanar, L., Stoj, C. S., Kosman, D. J. and Solomon, E. I.** (2007). Spectroscopic and kinetic studies of perturbed trinuclear

copper cluster: The role of protons in reductive cleavage of the O-O bond in the multicopper oxidases, *Journal of American Chemical Society*, **129**, 13118-13126.

[38] **Quintanar, L., Stoj, C., Wang, T., Kosman, D. J. and Solomon, E. I.** (2007). Role of aspartate 94 in decay of the peroxide intermediate in the multicopper oxidase Fet3p, *Biochemistry*, **44**, 6081-6091.

[39] **Agustine, A. J., Kjaergaard, C., Qayyum, M., Ziegler, L., Kosman, D. J., Hodgson, K. O., Hedman, B., and Solomon, E. I.** (2010). Systemic perturbation of trinuclear copper cluster in the multicopper oxidases: The role of active site asymmetry in its reduction of O_2 to H_2O, *Journal of American Chemical Society*, **132**, 6057-6067.

[40] **Gaussian 09, Revision A.02,** M. J. Frisch, G. W. Trucks, H. B. Schlegel, G. E. Scuseria, M. A. Robb, J. R. Cheeseman, G. Scalmani, V. Barone, B. Mennucci, G. A. Petersson, H. Nakatsuji, M. Caricato, X. Li, H. P. Hratchian, A. F. Izmaylov, J. Bloino, G. Zheng, J. L. Sonnenberg, M. Hada, M. Ehara, K. Toyota, R. Fukuda, J. Hasegawa, M. Ishida, T. Nakajima, Y. Honda, O. Kitao, H. Nakai, T. Vreven, J. A. Montgomery, Jr., J. E. Peralta, F. Ogliaro, M. Bearpark, J. J. Heyd, E. Brothers, K. N. Kudin, V. N. Staroverov, R. Kobayashi, J. Normand, K. Raghavachari, A. Rendell, J. C. Burant, S. S. Iyengar, J. Tomasi, M. Cossi, N. Rega, J. M. Millam, M. Klene, J. E. Knox, J. B. Cross, V. Bakken, C. Adamo, J. Jaramillo, R. Gomperts, R. E. Stratmann, O. Yazyev, A. J. Austin, R. Cammi, C. Pomelli, J. W. Ochterski, R. L. Martin, K. Morokuma, V. G. Zakrzewski, G. A. Voth, P. Salvador, J. J. Dannenberg, S. Dapprich, A. D. Daniels, O. Farkas, J. B. Foresman, J. V. Ortiz, J. Cioslowski, and D. J. Fox, Gaussian, Inc., Wallingford CT, 2009.

[41] **Babu, C. S. and Lim, C.** (2006). Emprical force fields for biologically active divalent metal cations in water, *Journal of Phys. Chem. A.*, **110**, 691-699.

[42] **D.A. Case, T.A. Darden, T.E. Cheatham, III, C.L. Simmerling, J. Wang, R.E. Duke, R. Luo, R.C. Walker, W. Zhang, K.M. Merz, B. Roberts, S. Hayik, A. Roitberg, G. Seabra, J. Swails, A.W. Götz, I. Kolossváry, K.F. Wong, F. Paesani, J. Vanicek, R.M. Wolf, J. Liu, X. Wu, S.R. Brozell, T. Steinbrecher, H. Gohlke, Q. Cai, X. Ye, J. Wang, M.-J. Hsieh, G. Cui, D.R. Roe, D.H. Mathews, M.G. Seetin, R. Salomon-Ferrer, C. Sagui, V. Babin, T. Luchko, S. Gusarov, A. Kovalenko, and P.A. Kollman** (2012), AMBER 12, University of California, San Francisco

[43] **Vreven, T., Byun, K. S., Komáromi, I., Dapprich, S., Montgomery, J. A., Morokuma, K. and Frisch, M. J.** (2006). Combining quantum mechanics methods with molecular mechanics methods ONIOM, *Journal of Chemical Theory and Computation*, **2**, 815-826.

[44] **Vreven, T., Morokuma, K., Farkas, Ö., Schlegel, H. B. and Frisch, M. J.** (2003). Geometry optimization with QM/MM, ONIOM, and other combined methods. I. Microiterations and constraints, *Journal of Computational Chemistry*, **24**:6.

[45] **Brooks, B. R., Bruccoleri, R. E., Olafson, B. D., States, D. J., Swaminathan, S. and Karplus, M.** (1983). CHARMM: A Program for Macromolecular Energy, Minimization, and Dynamics Calculations, *J. Comp. Chem*. **4**, 187-217.

[46] **Cramer, C. J.** (2002). Essentials of Computational Chemistry, Theories and Models, Minnesota, USA.

[47] **Zhao Y., Truhlar D. G.** (2008). The M06 suite of density functionals for main group thermochemistry, thermochemical kinetics, noncovalent interactions, excited states, and transition elements: two new functionals and systematic testing of four M06-class functionals and 12 other functionals. *Theor. Chem Account* 120:215–241.

[48] **Zhao Y., Truhlar D. G.** (2006). A new local density functional for main-group thermochemistry, transition metal bonding, thermochemical kinetics, and noncovalent interactions.*J. Chem. Phys*. 125:194101.

[49] **Liao, M. and Scheiner, S.** (2001). Electronic structure and bonding in phthalocyanines, metal=Fe, Co, Ni, Cu, Zn, Mn, *Journal of Chemical Physics*, **114**:22.

CURRICULUM VITAE

Name Surname: Erhan Özdamar

Place and Date of Birth: Zeytinburnu/İstanbul 17/02/1986

Address: Barış sok. No:4/25 34180 Bahçelievler/İSTANBUL

E-Mail: ozdamare@gmail.com

B.Sc.: Molecular Biology and Genetics, Istanbul Technical University, 2009

Professional Experience and Rewards:

Özdamar E. 2010. Genetiği Değiştirilmiş Organizmalar (GDO), Hava Kuvvetleri Dergisi 365:38-44

Çukuroğlu E., **Özdamar E**., Özkırımlı E., Keskin Ö. **2009**. Flexibility is a distinguishing property of hub proteins. Poster, Biophysical Society 2009, Boston, ABD.

(2011) TUBITAK BIDEB 2210 – Domestic Master Scholarship Program Student, October.

(2009) Dr. Yük. Müh. Orhan ÖCALGİRAY Academic Achievement Award of Molecular Biology and Genetics.

(2009) High Honour Degree in Molecular Biology and Genetics, Istanbul Technical University.